Evolutionarily stable gene clusters shed light on the common grounds of pathogenicity in the *Acinetobacter calcoaceticus-baumannii* complex

Bardya Djahanschiri[1], Gisela Di Venanzio[2], Jesus S. Distel[2], Jennifer Breisch[3], Marius Alfred Dieckmann[4], Alexander Goesmann[4], Beate Averhoff[3], Stephan Göttig[5], Gottfried Wilharm[6], Mario F. Feldman[2] and Ingo Ebersberger[1,7,8*]

1 Applied Bioinformatics Group, Inst. of Cell Biology and Neuroscience, Goethe University Frankfurt, Frankfurt am Main, Germany

2 Department of Molecular Microbiology, Washington University School of Medicine, St Louis, MO 63110, USA

3 Inst. of Molecular Biosciences, Goethe University Frankfurt, Frankfurt am Main, Germany

4 Bioinformatics and Systems Biology, Justus Liebig University Gießen, Gießen, Germany

5 Institute for Medical Microbiology and Infection Control, University Hospital, Goethe University, Frankfurt, Germany.

6 Robert Koch Institute, Project group P2, Wernigerode, Germany

7 Senckenberg Biodiversity and Climate Research Centre (S-BIKF), Frankfurt am Main, Germany

8 LOEWE Center for Translational Biodiversity Genomics (TBG), Frankfurt am Main, Germany

*Correspondence to: ebersberger@bio.uni-frankfurt.de

Abstract

Nosocomial pathogens of the *Acinetobacter calcoaceticus-baumannii* (ACB) complex are a cautionary example for the world-wide spread of multi- and pan-drug resistant bacteria. Aiding the urgent demand for novel therapeutic targets, comparative genomics studies between pathogens and their apathogenic relatives shed light on the genetic basis of human-pathogen interaction. Yet, existing studies are limited in taxonomic scope, sensing of the phylogenetic signal, and resolution by largely analyzing genes isolated from their functional contexts. Here, we explored more than 3,000 *Acinetobacter* genomes in a phylogenomic framework integrating orthology-based phylogenetic profiling and microsynteny conservation analyses. This allowed to delineate gene clusters in the type strain *A. baumannii ATCC 19606* whose evolutionary conservation indicates a functional integration of the subsumed genes. These evolutionarily stable gene clusters (ESGCs) reveal metabolic pathways, transcriptional regulators residing next to their targets but also tie together sub-clusters with distinct functions to form higher-order functional modules. We shortlisted 150 ESGCs that either co-emerged with, or are found preferentially in, the pathogenic ACB clade. They unveil, at an unprecedented resolution, the genetic makeup that coincides with the manifestation of the pathogenic phenotype in the last common ancestor of the ACB clade. Key innovations are the remodeling of the regulatory-effector cascade connecting LuxR/LuxI quorum sensing via an intermediate messenger to biofilm formation, the extension of micronutrient scavenging systems, and the increase of metabolic flexibility by exploiting carbon sources that are provided by the human host. Specifically, we could show that only members of the ACB clade use kynurenine as a sole carbon and energy source, a substance produced by humans to fine-tune the antimicrobial innate immune response. In summary, this study provides a rich and unbiased set of novel testable

47 hypotheses on how pathogenic *Acinetobacter* interact with and ultimately infect their
48 human host. They disclose promising routes for future therapeutic strategies.

49 ## Keywords

50 gene cluster, kynurenine, carbohydrate metabolism, phylogenomics, biofilm, quorum
51 sensing, synteny, virulence, innate immune response

52

53 ## Author Summary

54 The spread of multi- and pan-drug resistant bacterial pathogens is a world-wide threat to
55 human health. Understanding the genetics of host colonization and infection is essential for
56 devising novel ways of treatment. *Acinetobacter baumannii*, a nosocomial pathogen ranked
57 top by the World Health Organization in the list of bacteria for which novel therapeutic
58 approaches are needed, is a prime example. Here, we have carved out the genetic make-up
59 that distinguishes *A. baumannii* and its pathogenic next relatives comprising the *A.*
60 *baumannii–calcoaceticus* complex from other and mostly apathogenic *Acinetobacter*
61 species. We found a rich spectrum of pathways and regulatory modules that reveals how the
62 pathogens have modified biofilm formation, iron scavenging, and their carbohydrate
63 metabolism to adapt to their human host. Among these, the capability to metabolize
64 kynurenine is particularly intriguing. Humans produce this substance to contain bacterial
65 invaders and to fine-tune the innate immune response. But *A. baumannii* and its allies have
66 turned the table. They feed on kynurenine, and thus most likely also dysregulate human
67 immune response. In summary, our study substantially deepens the understanding of how a
68 highly critical pathogen interacts with its host, which substantially eases the identification of
69 novel targets for innovative therapeutic strategies.

70

Introduction

Acinetobacter is a physiologically and biochemically diverse genus of Gram-negative coccobacilli. Most of its species are considered benign, but the genus harbors with the *Acinetobacter calcoaceticus-baumannii* (ACB) complex a group of closely related human opportunistic pathogens [1, 2] that account for the vast majority of severe hospital-acquired *Acinetobacter* spp. infections [3-7]. *Acinetobacter baumannii*, a notorious nosocomial pathogen, is the most renowned member of the ACB complex and signs responsible for up to 5% of the total bacterial infections in hospitals worldwide [8]. By now, antibiotic resistance determinants against virtually all available antibiotics drugs are present in *A. baumannii* [9], and multi- or even pan-drug resistant strains are isolated from 44% of all patients with an *A. baumannii* induced infection [10]. At the same time, both the frequency and severity of infections have increased. Recent case studies report mortality rates of up to 70% [11-13] as well as growing numbers of (clonal) epidemic outbreaks [14]. Moreover, community-acquired infections by members of the ACB complex begin to rise [6, 15]. In recent years, significant advancements in the molecular characterization of drug resistance mechanisms have led to more informed drug administration schemes for hospitalized patients [6]. Still, the ease with which *A. baumannii* acquires resistance to novel antibiotics [10] makes it likely that resistant strains and their resistance determinants are going to spread at a faster pace than novel antimicrobials become available [16]. As a consequence, *A. baumannii* ranks top in the WHO charts of pathogens for which drug development is most urgent [17].

A systemic understanding of how *A. baumannii* interacts with and infects their human host can lead to novel paths for antimicrobial treatments [18-20]. Three main approaches have been used to elucidate the molecular basis of *Acinetobacter* virulence. Candidate approaches

(i) have scanned for virulence factors previously characterized in other bacterial pathogens [4, 7, 21-25]. To extend the scope beyond pre-compiled virulence factor catalogs, genome-wide approaches (ii) have assessed, for example, the effect of gene knockouts on the infection process (e.g. [12, 26]), or have identified the transcriptional changes under conditions the bacterium typically encounters in the human host (e. g. [23, 27]). These studies are, in theory, the most comprehensive way to identify virulence-related traits. However, experiments are usually performed only on a small set of model strains (e.g. [28]). Moreover, the limited set of tested conditions cannot reflect the diversity of infection sites in the human body. Consequently, results are hard to generalize. Lastly, factors that contribute only indirectly to virulence are hard to pinpoint. For example, we have only begun to understand how adaptations in the carbohydrate metabolism contribute to the virulence of *A. baumannii* [29]. Comparative genomics studies (iii) provided complementary evidence with the potential to overcome limitations imposed by the experimental procedures. They aim at identifying evolutionary changes that correlate with the emergence of pathogenic species [30]. To date, the genus *Acinetobacter* encompasses 72 (validly) named and mostly nonpathogenic species [31], which have been isolated from a broad range of habitats such as floral nectar, tree bark, seawater, but also animals [32]. This diversity provides an almost perfect setup to identify changes in the gene repertoires that are associated with the evolutionary emergence of the pathogenic potential, which eventually manifested in the ACB complex. Thus far, comparative genomics studies have begun to shed light on the general evolution of the genus [9] and the clonal epidemiology [33] of *A. baumannii*. They indicated that a major driver of *A. baumannii*'s success as a pathogen is its remarkably flexible genome [9]. High mutation rates [34] paired with the ability to acquire new, or alter the structure or expression of existing genes [11-13] promote a rapid adaptation to novel and adverse environmental conditions. Moreover, its

high genomic plasticity [34-36] facilitates the acquisition of antimicrobial resistance determinants complementing the intrinsic *A. baumannii* resistance [37]. However, against the intuition, most of the known virulence determinants were found also in the nonpathogenic members of the genus (e.g. [4, 38-40]). Thus, it is still largely unknown which genetic changes correlate with the emergence of the ACB complex as opportunistic human pathogens, and the genetic basis underlying the adaptation of *A. baumannii* to the human host largely remains to be understood [41].

Here, we exploit the availability of thousands of *Acinetobacter* spp. genomes in the public databases (NCBI RefSeq; [42]) to shed light on the evolution of the pathogenic ACB complex at a resolution that extends from a genus-wide overview to the level of individual clonal lineages within *A. baumannii.* For the first time, we integrate genus-wide ortholog searches, with analyses of gene order conservation providing a highly-resolved view on the joint evolutionary fate of neighboring genes using the type strain ATCC 19606 as a reference. This revealed 150 evolutionarily stable gene clusters ($ESGC_{ACB}$) that are prevalent in the ACB complex and rare or absent in the other members of the genus. The functional annotations of these ESGCs provide insights into the genetic and functional specifics of a clade comprising mostly pathogens, and thus direct the focus to key processes likely relevant for the adaptation of the bacterium to the human host. We find that the ACB complex acquired novel genetic modules for the regulation and formation of biofilms, for the scavenging of micronutrients, and have substantially extended their capabilities to exploit a diverse set of carbon sources. Most notably, we show that members of the ACB complex possess the kynurenine (Kyn) pathway and can grow on kynurenine as a sole carbon and energy source. The implications beyond the tapping of a novel carbon source are compelling. Both metabolites are produced by the human host via tryptophan degradation upon bacterial

143 infection and they contribute to the finetuning of the human innate immune response [43,
144 44]. Thus, the presence of the Kyn pathway allows members of the ACB complex to feed on
145 substances produced by the host to defend against bacterial attack. By that, they potentially
146 interfere with the kynurenine-dependent finetuning of the human innate immune response.

147 ## Results

148 The ability to infect humans emerged in the course of *Acinetobacter* spp. evolution and is a
149 hallmark of the ACB complex. Here, we exploited the full diversity of *Acinetobacter* genomes
150 available in the public databases that was available at the onset of the study (S1 Table). We
151 use this resource to trace changes in the *Acinetobacter* pan-genome that correlate with the
152 manifestation of pathogenicity in the ACB complex. To make the analyses computationally
153 tractable we devised a two-stage strategy.
154 In the priming stage, we determined the evolutionary relationships within the *Acinetobacter*
155 pan-genome with the orthology inference tool OMA [45]. Because the computational
156 complexity of the OMA ortholog search scales exponentially with the numbers of genes in
157 the pan-genome, we compiled a representative set of strains (Set-R) for this analysis. In
158 brief, we considered all available type, reference and representative genomes, as well as all
159 validly named species for which a genome sequence was available at the study onset. This
160 set was filled to a total number of 232 strains by adding further genomes to maximize the
161 phylogenetic diversity of the taxon set (see Methods, and S1 Text: Overview of genome
162 assemblies in Set-R). The corresponding strains together with genome assembly statistics,
163 and, where available, the origins of the isolates are summarized in S2 Table. Members of the
164 ACB complex harbor, on average, 14% more genes than other members of this genus
165 (students t-test - $p<0.001$; S1 Fig A). Gene counts were highly correlated with genome
166 lengths (spearman, $\rho=0.98$), and neither the difference in genome length nor the number of

encoded genes was significantly correlated with the assembly status (Completeness status "Complete" vs. Others, Kruskal-Wallis, p=0.311) (see S1 Fig B for further information). The Set-R pan-genome comprises 22,350 orthologous groups harboring 783,306 proteins; 16,000 proteins remained singletons (see S1 Fig C for a graphical representation). Rarefaction analyses revealed that the pan-genomes of the entire genus, the ACB complex, and *A. baumannii* are open (S1 Text: Pan-genome reconstruction). 889 genes represent the core genome of *Acinetobacter* (S3 Table; S1 Text: Core-genome reconstruction). Eventually, we tentatively annotated gene function in the Set-R pan-genome by linking the individual genes to COGs [46], to KEGG KOs [47], to entries in the virulence factor databases PATRIC [21] and VFDB [48], and by predicting their subcellular localization. To make this data available to the community, we developed the web application Aci-Dash (https://aci-dash.ingress.rancher.computational.bio/; Fig 1), the first web-based platform to interactively browse and explore the *Acinetobacter* pan-genome.

In the extension stage, we used a targeted ortholog search to complement the orthologous groups from the SET-R analysis with sequences from the remaining 2,820 *Acinetobacter* genomes (Set-F).

Consistency-based phylogeny of the genus *Acinetobacter*

To establish a stable phylogenetic backbone for our analysis, we reconstructed the maximum likelihood evolutionary relationships of the taxa in Set-R and Set-F, respectively, from three non-overlapping partitions of the 889 core genes. The majority-rule consensus phylogenies from the three trees each (Set-R – Fig 2A; Set-F – Fig 2B; for higher resolution versions see S2 Fig and S3 Fig, respectively) reveal that all named species (at the time of download) as well as the members of the ACB complex are consistently placed into monophyletic clades. Incongruencies between the three partition trees are confined to the

191 branching order within individual species, and here mainly within the densely sampled *A.*
192 *baumannii* and *A. pittii*. This indicates that genetic recombination, which is most likely the
193 source of the incongruent phylogenetic signal [49], is common enough only within species to
194 interfere with phylogenomic reconstructions based on hundreds of genes [50]. Across the
195 genus, we detected and corrected individual taxonomic assignments that are at odds with
196 the phylogenetic placement of the taxa, and most likely indicate mislabeled strains ([51,
197 52]). Specifically, we corrected 16 of such instances within the ACB clade, of which ten were
198 wrongly classified as *A. baumannii* according to NCBI RefSeq. In turn, 60 out of 182 genomes
199 with an unknown taxonomic assignment were placed within the ACB clade (see S4 Table for
200 species and clade assignments including the corrections). Interestingly, a comparison of the
201 average pair-wise nucleotide identity (ANI) across all genomes within Set-R revealed that at
202 least two genomes placed into the ACB clade cannot be associated with any known species
203 (ANI <95%, c. f. S4 Fig). This indicates that the full species diversity of the ACB complex is not
204 yet fully charted.
205 To ease the integration of the phylogenetic information into the following sections, we used
206 one species each to name the individual clades in the *Acinetobacter* phylogeny (Fig 2A).

207 ## Lifestyle and host switches during *Acinetobacter* evolution

208 The two earliest branching clades, named after *A. qingfengensis* (QI) and *A. brisouii* (BR),
209 respectively, solely comprise environmental species. *A. apis*, which was isolated from bees
210 [53], appears as an exception. However, *Acinetobacter* species are sporadically observed in
211 the bee gut, though they are not considered part of the gut microbiome [54]. Instead, they
212 likely represent environmental bacteria that were taken up by the bee with the food [55].
213 Thus, the capability to colonize animals evolved later and most likely in the ancestral species
214 prior to the split of the *A. lwoffii* (LW) clade (Fig 2B). Usually, members of the LW clade are

nonpathogenic. Repeated cases of human infection have only been reported for individual strains that mainly group with *A. lwoffii* and *A. radioresistens*, which manifested in vascular catheter-induced bloodstream infections with a low mortality rate [56]. Thus, human infection is likely an exception rather than the rule for this clade. Species descending from the most recent common ancestor *A. baumannii* shares with the *A. baylyi* clade (BA, in particular *A. ursingii*) and with the *A. haemolyticus* clade (HA), respectively, are found increasingly often associated with human pathogenicity, suggesting a progressive adaptation to humans as a host [57]. Members of the monophyletic ACB complex (ACB clade), which subsumes the *A. pittii clade* (PI), the *A. nosocomialis* clade (NO), and the *A. baumannii* clade (B), are all potentially pathogenic, although *A. calcoaceticus* has, thus far, very rarely been seen in the context of human infection. It can be speculated that the few reported cases were due to a miss-classified strain from a different species (see subsection "Consistency-based phylogeny of the genus Acinetobacter" above). Thus, *A. calcoaceticus* at least substantially reduced its pathogenic potential if not lost it completely [25].

Functional innovation in the Set-R pan-genome

We next scanned the Set-R pan-genome for gains of function on the lineage towards contemporary *A. baumannii*. We tentatively stratified the pan-genome by assigning each orthologous group to the inner node in the *Acinetobacter* phylogeny that represents the last common ancestor (LCA) of the two most distantly related taxa in that group (Fig 3A). For each node, we then determined the set of significantly enriched gene functions using the gene ontology (GO) terms from the sub-ontology Biological Process. Because genes with a sparse phylogenetic distribution cannot drive the shared phenotype of a clade, we confined the GO term enrichment analysis to only the subset of orthologous groups, where orthologs were detected in at least half of the subsumed taxa of a node (Fig 3B; Table 1; S5 Table). This

239 revealed several processes with potential relevance for pathogenicity, e.g. cell adhesion,
240 siderophore biosynthesis, and response to oxidative stress. However, reproducing previous
241 observations [4, 38-40], the corresponding genes were assigned to nodes in the phylogeny
242 that predate the emergence of the ACB clade. Only three significantly enriched GO terms
243 were assigned to the node representing the LCA of the ACB clade, and no term was
244 significantly enriched in the genes private to *A. baumannii*.
245

246 Table 1 Selection of overrepresented GO terms in the assigned gene sets of the inner nodes.[1]

Node	GO	Biological Process	p_cor[2]	RT[3]	RB[4]	d[5]	SC[6]	SA[7]	%B[8]	%ACB[9]	%nACB[10]
ACB+BR (n=230)	GO:0018189	pyrroloquinoline quinone biosynthesis	$<10^{-7}$	8.6	5.0	9	192	5	97.8	98.7	17.0
	GO:0006855	drug tm transport	$<10^{-7}$	2.4	9.5	5	53	1	96.4	96.8	23.4
	GO:0015810/3	aspartate/L-glutamate tm transport	$<10^{-7}$	4.3	2.5	10	96	2	96.4	97.8	24.8
	GO:0071705	nitrogen compound transport	$<10^{-7}$	2.8	9.1	4	62	1	100	100	27.7
	GO:0019439	aromatic compound catabolism	$5.2*10^{-3}$	2.2	14.0	4	49	2	92.7	95.7	28.4
	GO:0006631	fatty acid metabolism	$<10^{-7}$	3.3	6.5	7	73	1	89.1	91.4	36.2
	GO:0019619	3,4-dihydroxybenzoate catabolism	$<10^{-7}$	3.2	10.6	8	72	1	90.9	92.5	39.0
	GO:0007155	cell adhesion	$<10^{-7}$	4.6	10.6	2	103	1	98.2	98.9	40.4
	GO:0010124	phenylacetate catabolism	$<10^{-7}$	10.4	8.5	8	233	4	89.6	90.6	45.7
ACB+LW (n=223)	GO:0031388	organic acid phosphorylation	$<10^{-7}$	2.9	2.4	6	54	1	98.2	98.9	14.9
	GO:0009437	carnitine metabolism	$3.1*10^{-3}$	0.2	0.1	6	3	1	94.5	88.2	22.0
	GO:0071705	nitrogen compound transport	$<10^{-7}$	4.4	10.5	4	83	2	99.1	94.6	23.4
	GO:0036104	Kdo2-lipid A biosynthesis	$<10^{-7}$	2.4	3.8	8	45	1	94.5	91.4	29.8
	GO:0009435	NAD biosynthesis	$<10^{-7}$	3.4	15.7	11	65	1	89.1	91.4	30.5
	GO:0009116	nucleoside metabolism	$<10^{-7}$	3.5	13.0	6	67	1	96.4	95.7	31.2
	GO:0055085	tm transport	$<10^{-7}$	24.2	149.4	4	459	7	90.2	89.1	38.7
	GO:0019557/6	histidine catabolism to glutamate and formate/formamide	$<10^{-7}$	9.9	6.1	10	188	3	95.8	97.5	41.6
	GO:0006351	transcription, DNA-templated	$<10^{-7}$	86.9	320.1	9	1645	21	95.5	93.7	41.8
	GO:0019290	siderophore biosynthesis	$<10^{-7}$	8.0	4.8	8	170	3	95.8	72.8	41.8
ACB+BA (n=152)	GO:0045150	acetoin catabolism	$<10^{-7}$	33.6	0.8	7	36	1	100	100	14.9
	GO:0019290	siderophore biosynthesis	$<10^{-7}$	29.9	5.6	8	32	1	96.4	97.8	22.0
	GO:0006351	transcription, DNA-templated	$<10^{-7}$	76.5	0.03	9	82	2	84.5	84.9	26.2
ACB+HA (n=143)	GO:0022904	respiratory electron transport chain	$<10^{-7}$	45.9	5.39	5	44	0	90.9	79.6	11.3
	GO:0006351	transcription, DNA-templated	$<10^{-7}$	78.3	314.8	9	75	0	90.9	91.4	27.0
ACB (n=93)	GO:0009372	quorum sensing	$<10^{-7}$	8.8	0.3	3	13	2	86.4	90.3	0.0
	GO:0006351	transcription, DNA-templated	$<10^{-7}$	98.9	318.1	9	146	5	92.0	87.1	0.0
	GO:0006979	response to oxidative stress	$4.7*10^{-5}$	9.5	17.4	3	14	1	89.1	78.5	0.0

247

[1] The full list of enriched terms is provided in S5 Table 1.
[2] corrected p-value
[3] Ratio of genes with term in test set of that node ($\times 10^{-3}$)
[4] Ratio of genes in background set of that node ($\times 10^{-4}$)
[5] Depth of term in GO tree
[6] Count of subjects with term in study set of that node
[7] Number of ortholog groups associated with proteins in the study set. For this table, redundancy was reduced by selecting the lowest depth GO terms if any two GO terms had non-empty intersections between their sets of protein sequence identifiers or associated ortholog group identifiers.
[8] Mean prevalence of associated ortholog groups in *A. baumannii*
[9] Mean prevalence of associated ortholog groups in the ACB clade
[10] Mean prevalence of associated ortholog groups in *Acinetobacter* spp.

Evolutionary and functional units in the ATCC 19606 gene set

The GO term enrichment analysis revealed only a weak signal for the gain of biological processes that can be directly connected to bacterial virulence in the evolutionarily younger nodes of the *Acinetobacter* phylogeny. However, two factors confound the analysis. Only about two-thirds of all unique sequences in the *Acinetobacter* spp. pan-genome is annotated with a GO term and many of the genes with only unspecific terms. Moreover, the sporadic presence of orthologs to individual genes in taxa outside the ACB clade, e.g. as a result of recombination, confounds the phylogenetic stratification of the pan-genome. To increase both power and resolution, we widened the focus and traced the emergence and evolution of gene clusters in *Acinetobacter* spp. using the type strain *A. baumannii* ATCC 19606 as a reference. For each gene in the type strain, we integrated its node assignment, the abundance of orthologs within *A. baumannii*, within other members of the ACB clade, and within the remaining taxa in SET-R, respectively, and, where applicable, the overrepresented GO terms (Fig 4). As a recurrent theme, we observed that genes linked to the same overrepresented GO term reside adjacent to genes with highly similar phylogenetic abundance patterns, despite being occasionally assigned to different nodes in the phylogeny. We subsequently connected neighboring genes with significantly similar abundance patterns across the entire genome of *A. baumannii* ATCC 19606 to form candidate clusters. A candidate cluster was then propagated to represent an evolutionarily stable gene cluster (ESGC), which likely forms a functional entity if its gene order was found conserved within the ACB clade (S6 Table 3). Subsequently, we shortlisted 150 $ESGC_{ACB}$ that are abundant among members of the ACB clade and, at the same time, rare or even absent outside the clade (SE1.3 and SE1.4; see S1 Text: Workflow of ESGC identification and shortlisting). As the last step, we manually validated the automatic $ESGC_{ACB}$ assignment for

44 clusters whose sets of genes were each functionally annotated to a level that allowed us to infer general cluster function (Fig 5), and for further 10 clusters with an unknown function but that are almost exclusively found in the ACB clade (Fig 6). These 54 $ESGC_{ACB}$ can be broadly distinguished into four categories: The cluster comprises (i) a known operon or metabolic gene cluster (e.g., $ESGC_{ACB}$-0622, phenylacetate metabolism), (ii) a group of functionally related genes that are linked to genes, whose functional link, e.g. acting as a transcriptional regulator, was unknown thus far (e.g., $ESGC_{ACB}$-0162), (iii) super-clusters connecting two or more clusters with distinct functions to form a higher-order functional unit ($ESGC_{ACB}$-0394, *adeFGH* and *hisQMP*), and (iv) clusters of genes with an unknown function (e.g., $ESGC_{ACB}$-0503 to 0510; Fig 6). We hypothesize that the adaptation of pathogenic *Acinetobacter* species to their human host is likely mirrored in the various functions that these $ESGC_{ACB}$ convey. In the following sections, we highlight a selection of clusters related to persistence, micronutrient acquisition, and the evolution towards nutritional flexibility (see S1 Text: Gene clusters (ESGCs) not discussed in main manuscript).

The evolutionary emergence of the ACB clade coincides with changes in quorum sensing and biofilm formation

Quorum sensing and biofilm formation are key determinants of *A. baumannii* virulence [58-60]. Both functions are represented by $ESGC_{ACB}$-0162 (14 genes) and 0410 (8 genes). $ESGC_{ACB}$-0162 represents the regulatory module of this process. It harbors the Lux-type quorum sensing system (QS_{Lux}), which regulates motility and biofilm formation in *A. baumannii,* and additionally, a biosynthetic gene cluster containing a non-ribosomal peptide synthetase here referred to as NRPS cluster. Both genes of QS_{Lux}, *abaI* and *abaR,* are separated by a short gene that was tentatively named *abaM* (Fig 7A; see also S1 Text: Characterization of AbaM). This three-gene architecture is conserved in the ACB clade, and it

296 is common in *Burkholderia* spp. [61], where the intervening short gene acts as a negative
297 regulator of the QS_{Lux} system [62]. Recently, initial evidence emerged that AbaM in the *A.*
298 *baumannii* strain AB5075 indeed regulates quorum sensing and biofilm formation [63]. In
299 the light of our results, we propose that AbaM is an understudied modulator of quorum
300 sensing in the entire ACB clade.
301 The NRPS cluster (Fig 7A) produces a three-amino acid lipopeptide, Ac-505 [60], which likely
302 plays a central role in regulating bacterial motility and biofilm formation [64]. Disrupting its
303 biogenesis alters the expression of numerous factors involved in biofilm formation and
304 surface adherence [65], in particular the chaperon-usher pili (CUP) and the archaic
305 chaperon-usher pili (CSU). Consequently, host cell adhesion and virulence of *A. baumannii*
306 are substantially reduced. Here, we provide first-time evidence that the evolutionary fate of
307 the NRPS cluster is intimately intertwined with that of the QS_{Lux} cluster. We found that the
308 rare strain-specific loss of the QS_{Lux}-cluster determines the loss of the NRPS cluster, which
309 implies that they not only form an evolutionary but also a functional unit. Interestingly,
310 strains lacking $ESGC_{ACB}$-0162 are not randomly distributed. Most prominently, the cluster is
311 missing in almost all (48/55) *A. baumannii* strains representing the international clone type
312 (IC) 8 (Fig 5). The formation of a higher-order module comprising the QS genes and an NRPS
313 biosynthetic gene cluster is a repeated scheme during bacterial evolution. For example, the
314 methane-oxidizing bacterium *Methylobacter tundripaludum* harbors an NRPS biosynthetic
315 gene cluster that was integrated between the *abaI* and *abaR* orthologs. And the production
316 of the corresponding extracellular factor is under control of the QS cluster [66]. NRPS-
317 dependent molecules have been implicated to mediate interspecific communications across
318 kingdoms both in symbiotic and pathogenic communities. In *P. aeruginosa*, the interplay of
319 N-acyl-L-homoserine lactone-dependent quorum-sensing signaling and an NRPS-dependent

biosynthesis of bacterial cyclodipeptides (CDPs), which act as auxin signal mimics, modulates the communication to its host plant *Arabidopsis thaliana* [67]. It can be speculated that $ESGC_{ACB}$-0162 may similarly coordinate, the communication between the bacteria and their human host.

$ESGC_{ACB}$-0410, harbors the Csu cluster responsible for biofilm formation on abiotic surfaces via archaic chaperon-usher pili [68, 69] (Fig 7B) together with a transcriptional regulator of the TetR/AcrR family (TFTRs) (S5 Fig id:0410). TFTRs represent one-component systems that regulate a broad variety of cellular processes in bacteria, among them many that are related to virulence such as efflux pump expression and biofilm formation [70, 71]. Notably, they are often encoded alongside their target operons. To the best of our knowledge, regulation of the Csu cluster via an adjacent TFTR has never been reported. Thus, next to the two-component systems BfmRS [72] and GacSA [73], a third hitherto undescribed one-component system, seems to be involved in regulating the formation of Csu pili.

In line with our finding that $ESGC_{ACB}$-0162 and $ESGC_{ACB}$-0410 have similar abundance patterns (cf. Fig 5), the regulation of the Csu cluster appears under the direct control of Ac-505 [26, 65]. Thus, Ac-505 likely acts as a modulator between biofilm formation on abiotic and biotic surfaces. However, contrary to the QS_{Lux} - NRPS supercluster, the Csu cluster was lost multiple times independently in the ACB clade (Fig 5). Given its terminal position in the regulator-effector cascade, this indicates a lineage-specific fine-tuning of biofilm formation.

Interestingly, within *A. baumannii*, we find that all 55 IC8 strains in our dataset lack both the QS_{Lux} - NRPS supercluster and the Csu cluster, which points towards substantial changes in the way how IC8 strains regulate biofilm formation.

KatA – an ACB clade specific catalase

The genome of *A. baumannii* ATCC 19606 harbors five putative catalases: *katA*, *katE*, *katE-like*, *katG*, and *katX* [23, 74]. Note, that both Sun et al. [74] and Juttukonda et al. [23, 74] refer to a catalase labeled *katE*, which, however, represent different genes (locus tags A1S_1386/A1S_3382 and DJ41_RS22765/DJ41_RS10660 in *A. baumannii* ATCC 17978 and ATCC 19606, respectively). We, therefore, named the latter *katE*-like. *KatA* is the only catalase that is exclusively found in the ACB clade. The corresponding gene resides in a cluster next to a putative MFS transporter and a cytochrome b561 ($ESGC_{ACB}$-0624, Fig 7C). The KatA cluster is highly conserved in all species of the ACB clade except *A. calcoaeceticus*, where it has been lost (cf. Figs 5 and 7C). Upon host infection, both neutrophils and macrophages recruit radical oxygen species (ROS) for bacterial clearance [75, 76], and thus ROS defense mechanisms are an essential contributor to bacterial virulence. However, an initial investigation in *Ab* ATCC 17978 found no obvious link between KatA and ROS protection [23]. Still, the abundance pattern of $ESGC_{ACB}$-0624 is perfectly in line with the hypothesis that this cluster contributes to virulence in pathogenic members of the ACB clade, and more comprehensive studies are needed to elucidate its precise role during bacterial infection.

Metabolic adaptation – Micronutrient acquisition is refined in the ACB-clade

All members of the genus *Acinetobacter* must supply their demand of essential micronutrients, most importantly iron and zinc. Acquisition systems for these two metals are therefore represented in the genus-wide core genome (Fig 8). However, both iron and zinc are actively sequestered by the host to starve invading pathogens, a strategy referred to as nutritional immunity [77]. This likely results in a strong selective pressure for the pathogenic

365 ACB clade to optimize scavenging systems such that the reduced bioavailability of these
366 metal ions in the host can be counterbalanced.
367 Acquisition systems for iron, whose limited availability at the host-pathogen interface is
368 considered one of the key obstacles for invading and persisting within the human host, are a
369 showcase example. The iron transporter system *feoABC* represents the evolutionary core of
370 iron uptake. It is complemented, in many but not all taxa [28] both inside and outside of the
371 ACB clade, by the baumannoferrin cluster (Fig 8). Two further clusters extend the spectrum
372 of iron uptake systems exclusively in the ACB clade. $ESGC_{ACB}$-0498 represents the 2,3-
373 dihydroxybenzoic acid synthesis cluster (*entAB*), which synthesizes a siderophore precursor
374 [78]. $ESGC_{ACB}$-0368 and 0369 together resemble the acinetobactin biosynthesis clusters
375 *bauA-F*, *basA-I* and *barAB*. However, a third cluster, $ESGC_{ACB}$-0485, that very likely represents
376 an ABC-type Fe^{3+}-hydroxamate transport system seems to extend the diversity of iron
377 uptake systems in the ACB clade even further. It encodes a substrate-binding protein, an iron
378 complex ABC transporter (permease), an ATP-binding protein, and an N-Acetyltransferase
379 protein (GNAT family). The AraC-family-like transcriptional regulator, which is located
380 downstream on the opposite strand in $ESGC_{ACB}$-0485, likely controls the expression of this
381 cluster. In line with this operon-like organization, these genes are jointly downregulated
382 under mucin-rich conditions [79]. The complex and seemingly redundant infrastructure for
383 iron uptake in the ACB clade seems at odds with a recent study in *A. baumannii* ATCC 17978,
384 which stated that acinetobactin is the only system that is necessary for *A. baumannii* to grow
385 on host iron sources [80]. However, here we show that this conclusion does not generalize
386 to the entire ACB clade. The pathogens *A. nosocomialis* and *A. seifertii*, for example, lost the
387 acinetobactin cluster (cf. Fig 5). Instead, it is conceivable that the diversity of iron acquisition

388 systems is an adaptation to diverse niches each requiring different strategies of iron
389 scavenging.
390 Given the essentiality of zinc (Zn), it is not surprising to see that also Zn uptake was refined
391 on the lineage towards the ACB clade. The zinc uptake system Znu, including the distal *znuD*
392 gene, which facilitates resistance to human calprotectin-mediated zinc sequestration [23], is
393 evolutionarily old and part of the genus-wide core genome (Fig 8) The histidine utilization
394 (Hut) system (*hutCDUHTIG*, $ESGC_{ACB}$-0215) is prevalent in the ACB clade, though not
395 exclusively. This system ensures the bio-availability of Zn via the histidine catabolism both
396 under high availability and starvation of Zn. However, it requires histidine to be abundant.
397 Interestingly, the most recent acquisition in the Zn metabolism is the putative
398 metallochaperone, ZigA. The corresponding gene resides directly adjacent to $ESGC_{ACB}$-0215,
399 and thus is likely an evolutionary more recent extension of this cluster. *zigA* was found active
400 only under Zn starvation, where it increases the bioavailability of Zn also under histidine
401 depletion [81] and counteracts nutritional starvation.
402 Manganese (Mn^{2+}) is required only in small amounts and is mostly used for coping with
403 reactive oxygen species (ROS), as Mn^{2+}, other than Fe^{2+}, does not promote the Fenton
404 reaction that converts H_2O_2 to highly damaging hydroxyl radicals [82, 83]. Therefore, Mn
405 uptake systems should be prevalent in bacteria frequently exposed to ROS stress,
406 particularly in the pathogenic *Acinetobacter* strains. Thus far, only one Mn acquisition
407 system, *mumRTLUHC* [84], has been identified in *Acinetobacter spp*. This system is
408 represented by $ESGC_{ACB}$-0611 and plays an essential role in protecting *A. baumannii* against
409 calprotectin-mediated Mn depletion by the host and contributes to bacterial fitness in a
410 murine pneumonia model [84]. $ESGC_{ACB}$-0611 is found throughout the genus though less
411 frequently in clades that are more distantly related to the ACB clade (cf. Fig 5 and 8). Within

412 the HA-clade, several species including *A. tjernbergiae*, *A. junii*, *A. beijnerickii,* and *A.*
413 *haemolyticus* lack both the putative manganese transporter gene *mumT* and the gene
414 encoding a putative hydrolase *mumU* (S5 Fig id:0611). Within IC 3, several strains lack the
415 entire cluster. These taxa either found alternatives to Mn^{2+}-dependent processes for coping
416 with oxidative stress, are more vulnerable to ROS, or they scavenge Mn^{2+} via a mechanism
417 that is still hidden in functionally uncharacterized gene clusters.
418 In summary, we see a clear signal that the ACB clade is enriched for genes and gene clusters
419 that functionally complement the genus-wide available and evolutionarily old metal uptake
420 systems. In line with the reinforcement hypothesis, these more recently acquired clusters
421 seem particularly important for metal scavenging during infection, i.e. when the metals are
422 actively sequestered by the host [80, 81].

423 ## Carbohydrate metabolism - Evolution towards nutritional flexibility

424 The ability of individual *Acinetobacter* strains to utilize a broad spectrum of carbon sources is
425 important for their adaptation to different environments, including the human host [40, 85-
426 88]. However, it is largely unknown when the corresponding metabolic pathways were
427 acquired during *Acinetobacter* evolution, how widespread they are, and if and to what
428 extent they are connected to the pathogenicity of the ACB clade. More than 20 of the
429 shortlisted $ESGCs_{ACB}$ represent pathways that shuttle metabolites into the carbohydrate
430 metabolism of the bacterium (Fig 5, in red font, and see Fig 9 for a selection), many of which
431 are prevalent in the human body. The corresponding gene clusters mostly channel these
432 metabolites into catabolic processes (see below). However, the genes involved in the
433 glucose/gluconate metabolism seem to fuel anabolic processes.

Glucose / Gluconate metabolism

Glucose and gluconate serve as carbon and energy sources for individual species in the genus *Acinetobacter*, e.g., *A. soli, A. apis,* and *A. baylyi.* For *A. baylyi* ADP1 it was shown that the glucose catabolism involves the Entner-Doudoroff pathway [89]. Members of the ACB clade have lost the ability to use glucose as a carbon source [90] (see also S6 Fig C and S7 Table). It is, thus, surprising that we find the genetic infrastructure to feed both molecules into the bacterial metabolism almost exclusively in the ACB clade.

$ESGC_{ACB}$-0112 comprises the gluconate permease (GntP) that shuttles gluconate from the periplasm into the bacterial cell (Fig 9, yellow pathway). The cluster further encodes the kinase GntK, which phosphorylates gluconate into 6-phosphogluconate, and the enzymes Edd and Eda of the Entner-Doudoroff pathway, which link to the pentose phosphate pathway that produces pyruvate. Members of the ACB clade also possess two variants of a glucose dehydrogenase (*gdh*), which catalyze the reaction from D-glucose to D-gluconate in the periplasm [91]. The membrane-bound variant (*gdhA*), forms together with an outer membrane porin a cluster of two genes, $ESGC_{ACB}$-0287 (cf. S1 Data id:0287), which is ubiquitous across *Acinetobacter* spp. We note that the porin is orthologous to OprB in *P. aeruginosa*, where it facilitates the diffusion of various sugars - including glucose - into the periplasm. The second, soluble Gdh (*gdhB*) is confined to and nearly ubiquitous in the ACB clade (S7 Fig, S6 Table 1, id:HOG3408).

The prosthetic group for both Gdh, pyrroloquinoline quinone (PQQ), is a small, redox-active molecule that serves as a cofactor for several bacterial dehydrogenases. $ESGC_{ACB}$-0497 comprises six genes that together represent the PQQ biosynthesis pathway: *pqqABCDE* and an additional membrane-bound dipeptidase referred to as *pqqF* in *Klebsiella pneumoniae* [92] (cf. Fig 9, pink). All genes reside contiguously on the same strand suggesting an operonic

structure. The complete cluster is present in almost all genomes of the ACB clade, although we had to manually confirm the presence of *pqqA*, because its length (40 amino acids) is below the length cutoff of the ortholog assignment tool. Only 31 out of 2436 strains in the ACB clade have lost the ability to synthesize PQQ, among them the model strain *A. baumannii* ATCC 17978. Cluster abundance outside the ACB clade is low (<20%), but it is present in all strains of species with demonstrated ability to assimilate glucose and gluconate (i.e. *A. soli*, *A. baylyi*, and *A. apis*, cf. [90]; SE2.0497).

The holoenzymes *GdhA* and/or *GdhB*, in theory, could establish a gapless route for glucose via this gluconate 'shunt' into the cell for further degradation via the Entner-Doudoroff pathway, even in the absence of a dedicated Glucose transporter. Why then does none of the tested strains in the ACB clade grow with glucose as sole carbon and energy source? We hypothesize that they utilize this route for anabolic processes exclusively, e.g. for the production of polysaccharides as it was demonstrated for *P. aeruginosa* [93].

Carbohydrate Catabolism

The ACB clade has substantially increased its repertoire of catabolic pathways for alternative carbon sources compared to taxa outside this clade [94]. For a small number of mostly hand-picked *A. baumannii* strains, previous studies have experimentally confirmed the ability to grow on tricarballylate and putrescine, malonate, butanediol and acetoin, phenylacetate, muconate, glucarate, galactarate (mucate), and 4-hydroxyproline as sole carbon sources [40, 85]. Our analyses identified the corresponding gene clusters among the $ESGC_{ACB}$. Hence, the ability to use these resources is prevalent in the ACB clade, whereas non-ACB species have to rely largely on different carbon sources. We will highlight two examples that likely represent an adaptation to humans as a host.

D-glucarate (saccharate) is a major organic acid in human serum [95]. $ESGC_{ACB}$-0568 comprises all necessary genes for glucarate and galactarate (mucic acid) degradation (Fig 9). In *Salmonella enterica* serovar Typhimurium deletion of the D-glucarate/D-galactarate permease ortholog attenuated virulence [96]. Further, galactarate digestion was shown to increase the colonization fitness of intestinal pathogens in antibiotic-treated mice and to promote bacterial survival during stress [97]. Given that $ESGC_{ACB}$-0568 is almost exclusively confined to the ACB clade, it is conceivable that this cluster contributes to colonization and virulence in pathogenic *Acinetobacter* species. It is therefore interesting that within *A. baumannii* the cluster is almost absent in IC2 strains (0.08% prevalence in Set-F; *cf.* Fig 5).

Carnitine is essential for the oxidative catabolism of fatty acids in humans [98]. $ESGC_{ACB}$-0016 comprises six genes necessary for catabolizing carnitine [99]. A LysR-type transcriptional regulator likely controls the activity of this cluster. The remaining five genes represent a putative tartrate dehydrogenase (*ttuC*), a BCCT-family carnitine transporter (Aci01347), a generically annotated alpha/beta hydrolase which possibly catalyses the conversion of D-acylcarnitine into L-carnitine (see Fig 9, green), and the genes encoding the two subunits of the carnitine monooxygenase CntA and CntB. The latter two genes are separated by a gene that is tentatively annotated as an NAD-dependent succinate-semialdehyde dehydrogenase. However, two lines of evidence indicate that the precise function of this gene as well as that of the putative tartrate hydrogenase might both differ. In the literature, the putative succinate-semialdehyde dehydrogenase is speculated to act as malic semialdehyde dehydrogenase [99], an enzyme that converts malate semialdehyde into malate. Further, the putative tartrate dehydrogenase belongs to the KEGG orthologous group KO7246 which is annotated as a D-malate dehydrogenase. The product of the latter enzyme, pyruvate, can be further processed into oxaloacetate, which serves as a substrate for the tricarboxylic acid

(TCA) cycle (cf. Fig 9). Assuming that the putative malic semialdehyde dehydrogenase produces D-malate, then, in the presence of an appropriate transporter, this cluster should allow the members of the ACB clade to utilize D-malate as a carbon source. We tested this hypothesis, and confirmed that *Ab* ATCC 19606 indeed grows on D-malate (S6 Fig B), which corroborates initial growth experiments [100]. We note that the unusual production of the D-malate enantiomer rather than L-malate would have a further interesting implication. It potentially allows the bacterium to accumulate D-malate in conditions when carnitine is abundant, without interfering with the stoichiometry of the remaining substrates of the TCA cycle.

Thus far, two *A. baumannii* strains have been shown to use carnitine as sole carbon source [101]. We evaluated exemplarily that the absence of the cluster indeed correlates with *Acinetobacter* inability to grow on carnitine and is not functionally complemented by an alternative degradation pathway. Both, *A. baylyi* ADP1 and the *A. calcoaceticus* type strain (DSM 30006), which both lack the $ESGC_{ACB}$-0016, did not grow on carnitine after 24h.

The clusters abundance profile reveals that the ability to metabolize carnitine occurs also outside the ACB clade (31 strains in Set-R; cf. Fig 5). However, 25 of these strains were isolated from infected patients, 2 from hospital sewage water, and only 3 strains were sampled from the environment (cf. S8 Table). The isolation origin of the one strain is unknown. The presence of the carnitine cluster, therefore, correlates surprisingly well with the pathogenic potential of a strain and it will be interesting to test a causal dependence. In support of causality, we find that the carnitine cluster is absent in *A. calcoaceticus*, the only species of the ACB clade that is nonpathogenic or at least has substantially reduced virulence (cf. S1 Text: $ESGC_{ACB}$-0016).

Novel carbon sources

The functional annotations of the $ESGC_{ACB}$ in Fig 5 indicate that the list of potential carbon sources for *A. baumannii* and other members of the ACB clade is still incomplete. We find degradation pathways for xanthine, 2-aminoethylphosphonate, acyclic terpenes, vanillin/valinate, taurine, and anthranilate (see S1 Text: Gene clusters (ESGCs) not discussed in main manuscript). To the best of our knowledge, none of these metabolites have been considered as potential carbon sources for *A. baumannii,* although a putative Xanthine dehydrogenase has been characterized previously via heterologous expression in *E. coli* [102]. One cluster is, however, particularly interesting because it intertwines the bacterial carbohydrate metabolism with the human tryptophan catabolism. $ESGC_{ACB}$-0452 (Fig 10A) harbors the kynurenine hydrolase KynU, which catalyzes the cleavage of kynurenine to anthranilic acid and alanine (Fig 10B). Within the same cluster, we identified an AsnC-type transcriptional regulator, a putative amino acid permease, and a gene generically annotated as an alpha/beta-hydrolase. Notably, this hydrolase is listed as an ortholog to the human kynurenine formamidase (KynB) in the OMA database [103] with which it shares the same domain architecture (Fig 10C). Together with its evolutionarily stable localization in the vicinity of KynU, this provides convincing evidence that the *A. baumannii* hydrolase resembles a hitherto overlooked KynB. This enzyme transforms formyl-kynurenine into kynurenine and, thus, acts immediately upstream of KynU in the Kynurenine pathway of tryptophan degradation (*cf.* Fig 10B). A similar gene cluster was recently described in *P. aeruginosa* (Pae) [104, 105], however with two notable exceptions: $KynB_{Aba}$ is substantially more similar both in sequence and domain architecture to the human KynB than the $KynB_{Pae}$ (Fig 10C), and we found no trace of an enzyme that catalyzes the formation of N-formyl-kynurenine from tryptophan in *A. baumannii*.

We next confirmed that the presence of the kynurenine cluster allows *A. baumannii* to grow on kynurenine as a sole carbon- and energy source (Fig 10D). A deletion of the Kyn-cluster abolished growth on kynurenine but not on anthranilate, the product of KynU (Fig 10D). In a last step, we investigated the phylogenetic profile of the Kyn-cluster in greater detail (Fig 10E and S2 Data). Within *Acinetobacter*, the cluster is almost exclusively present in the pathogens of the ACB clade, and it has been lost several times independently within *A. calcoaceticus*. Along the same lines, we find the Kyn-cluster in a proteobacteria-wide screen across more than 1,000 species (see S9 Table for the list of genomes and identifiers) only in a few taxa, of which many are opportunistic human pathogens (SF5). Taken together, our findings provide strong evidence that members of the ACB clade possess the genetic infrastructure to interfere with the tryptophan metabolism of humans, as it was already shown for *P. aeruginosa* [105]. This opens up a novel and hitherto unexplored route of how these pathogens interacts with its human host.

Discussion

In contrast to more virulent bacteria, the opportunistic nosocomial pathogens from the genus *Acinetobacter* pursue a resist-and-persist strategy [25]. Instead of pinpointing individual key determinants of bacterial virulence, this requires the unraveling of a likely broad and less specific genetic basis conveying adaptation to clinical environments and, at the same time, to the human host. Experimental studies, either *in vitro* bringing the advantage of controlled experimental conditions, or *in vivo* with the advantage of a realistic infection model have provided fundamental insights into the pathobiology of *Acinetobacter* [19, 20, 40]. However, pathogens encounter – and therefore have to adapt – to diverse environments during host infection [106]. The resulting selective landscape is complex, and therefore hard to reproduce in an experimental setup. Virulence determinants that are

576 relevant only under specific conditions or whose functions blend in with the bacterial
577 metabolism are easy to miss. Evolutionary approaches can close this gap. They focus on the
578 signal if a gene or a gene cluster likely contributes to pathogenicity, reflected by their
579 prevalence preferentially in pathogens, independent of the precise conditions when it is
580 active. Here, we have charted the genetic specifics of the pathogenic ACB clade at a
581 resolution ranging from a genus-wide overview down to individual clonal lineages within *A.*
582 *baumannii*. To ease the future integration of evolutionary evidence with functional studies,
583 we have developed the *Acinetobacter* dashboard Aci-Dash. This is the first web application
584 that allows the community to mine the abundance profiles of genes encoded in 232
585 representative genomes together with their functional annotations and their connection to
586 virulence factors.
587 Comparative genomics studies across the genus *Acinetobacter* have been performed before
588 (e.g. [9, 107]). The integration of orthology assignments with shared synteny analyses at a
589 scale that spans several thousand *Acinetobacter* genomes is yet unprecedented. The $ESGC_{ACB}$
590 detected here form relevant starting points for further unravelling the regulatory and
591 functional network in a human pathogen. They result in a rich set of testable hypotheses
592 whose experimental validations will likely deepen the understanding of the genetic basis of
593 *Acinetobacter* pathogenicity. Moreover, the lineage specific absence of ESGC within the
594 pathogenic clade, most prominently demonstrated by the loss of the QS-NRPS cluster
595 together with the Csu cluster in the IC 8, or of several clusters in *A. calcoaceticus*, helps to
596 better predict in which characteristics individual strains, clonal lineages, and species differ
597 from the prototype of an *Acinetobacter* pathogen.
598 The functions conveyed by these clusters are diverse and many can be readily connected to
599 *Acinetobacter* pathogenicity: Quorum sensing and biofilm formation [93], ROS response

[108], and micronutrient acquisition [77]. On top of these, the abundance of gene clusters involved the carbohydrate metabolism, a largely uncharted area of *Acinetobacter* virulence factors [29], strongly suggests that members of the ACB clade follow a general evolutionary trend towards greater metabolic flexibility, which is common to many bacterial pathogens [30, 106]. Such generalists have a selective advantage over niche-specialists in environments that are frequently disturbed or altered [109].

Metabolic interaction with the host, in particular those involving amino acids, have an interesting further implication, that has thus far not been considered in the context of *Acinetobacter* pathogens. They can modulate regulatory systems involved, for example, in the finetuning of the host immune response [30, 110]. The Kynurenine (Kyn) pathway detected in this study is a likely example of this connection. This cluster is almost entirely confined to the pathogenic members of the ACB-clade. Interestingly, and in contrast to the human pathogen *P. aeruginosa,* which also harbors a Kyn pathway, the key enzyme, IDO (KynA), that allows the bacteria to directly metabolize tryptophan via the kynurenine pathway is missing (cf. Fig 10B). How then do they fuel this pathway? Interestingly, tryptophan depletion via the kynurenine pathway is an important human immune defense mechanism upon bacterial infection [111]. Here, we provide first time evidence that pathogenic *Acinetobacter* species from the ACB clade can use the intermediate metabolites of the host response as additional carbon- and energy sources, likely further promoting its growth. However, the ability to degrade the intermediates of the human tryptophan catabolism has a further interesting implication for in the host-pathogen interaction. While it was shown that *P. aeruginosa* produces elevated levels of kynurenine to inhibit ROS production and aid bacterial survival [112], *Acinetobacter* species in possession of the Kyn cluster must pursue a different strategy. By scavenging kynurenine from their environment,

they can potentially interfere with the homeostasis of the human immune system, in particular with its suppressive effect on T cells and Natural killer cells. This potentially leads to host tissue damage due to the now uncontrolled production of ROS [76, 79]. Though at a high cost, this would allow the bacteria to use the rich nutrient resources enclosed in the host cells.

In summary, antimicrobial resistance is one of largest threats to global health. On the example of *Acinetobacter*, we have shown that the incorporation of a broad evolutionary perspective can pinpoint individual genes or entire pathways that result in novel and viable hypotheses of how the bacteria persist, feed off and interact with the host. At an early phase of drug development, these candidates provide promising anchor points from which the development of new therapeutic strategies to either prevent or treat *Acinetobacter* infections can be initiated.

Methods

Data Acquisition

The full data set (Set-F) comprises all assemblies in the NCBI RefSeq data base (version 87) stating 'Acinetobacter' in the 'organism' field [S1 Table]. From Set-F, we selected in total 232 representative strains covering all available type, reference and representative genomes, as well as all validly named species (https://apps.szu.cz/anemec/Classification.pdf) for which a genome sequence was available at the study onset are represented. We further picked genomes of several *A. baumannii* strains that are of interest due to e.g., their context of isolation as well as representatives of eight international clone types. Lastly, we included genomes from Set-F into Set-R that allow for an increase of the fraction of total phylogenetic

diversity covered without compromising the quality (cf. S1 Text: Taxon Set Construction). An overview of Set-R is provided in S2 Table.

To compile the *Proteobacteria* data set (n=1363), we selected all *Proteobacteria* represented in NCBI RefSeq data base (version 204) and selected one representative per species, which was either annotated as “reference” or “representative” strain.

International Clone Type (IC) and MLST assignments

For all strains in Set-F, we determined the sequence type with MLSTcheck v2.1.17 [113] using two different schemes, Oxford [114] and Pasteur [115], that were obtained from the PubMLST website (http://pubmlst.org/abaumannii/). All members of the *A. baumannii* clade were assigned to an international clone (IC) type whenever we found literature evidence that the predicted sequence types and IC were unambiguously linked using the following publications as a source: [35, 115-124]. The final assignments are provided in S1 Table and S2 Table based on strain typing results provided in S11 Table.

Phylogenetic diversity

Phylogenetic diversity scores of SET-F and SET-R were computed with PDA v.1.0.3 [125] using the options *-k=234:3027* and *-if=handpicked.list* based on the ML tree of SET-F. 25 low quality assemblies were pruned prior to this analysis to avoid overestimation because of long branches resulting from sequencing errors. A detailed description of the quality assessment is provided in S1 Text: Taxon Set Construction.

Average Nucleotide Identity

All genome sequences within Set-R were pair-wise aligned with Nucmer v3 [126], and the Average Nucleotide Identities (ANIm) were calculated with the script average_nucleotide_identity.py from the Python package pyani v0.2.7 [127] using the following options*: -i ./genomes -o ./output/ -m ANIm -g --gmethod seaborn –maxmatch*.

Ortholog Search

All against all orthology searches were performed with OMA standalone v.2.2.0 [45] and default parameter settings, except for decreasing the minimum length threshold for sequences considered (MinLen) to 40 residues. Targeted ortholog searches were performed with fDOG [128] using the OMA orthologous groups from SET-R to train the profile hidden Markov models.

Inference of the pan and core gene sets (SET-R)

The pan-genome size was calculated as the sum of the number of OGs and number of strain specific proteins (i.e. proteins without orthologs). For the rarefaction analysis, we identified the number of new orthologs and singletons per added genome in Set-R. The core genome was defined as the subset of OGs where each taxon of Set-R contributed exactly one ortholog. However, the strict definition of the core genome, yielded very small core genome estimates due to qualitative differences and incomplete draft genomes (S1 Text: Table 1). We therefore relaxed the core genome definition and allowed a core-gene to be absent in 1% of the genomes (max. 3 out of the 232) in Set-R (see S1 Text for further details). To obtain these values as a function of the number of genomes considered, we simulated a sequential inclusion of genomes in SET-R. Following the approach from Tettelin et al. [129], Pan- and core genome sizes were extrapolated by fitting the power law function $yP = \kappa Pn^{\gamma} + c$ and an exponential decaying function $yc = \kappa c \exp[-n*\tau c] + \Omega$, respectively, with nonlinear least-squares (Levenberg–Marquardt algorithm). Given the large taxon set in our study, we limited the simulation to 100 random permutations of a sequential inclusion.

Phylogenetic tree reconstruction

SET-R: Multiple sequence alignments (MSAs) for each orthologous group were generated with MAFFT-LiNSI [130] (v7.394, default parameters). Next, each protein's CDS was obtained

and PAL2NAL v14 [131] with the option *-codontable 11* was employed to infer protein sequence guided nucleotide MSAs. Supermatrices built from concatenated MSAs served as input for the maximum likelihood (ML) tree reconstruction. The best fitting substitution model (GTR + empirical base frequencies + free rate heterogeneity with 10 categories) was determined using IQ-Tree v1.6.8 [132] using the option *-m TEST*, and the following parameters were used for the ML tree reconstruction with IQ-Tree: *-m GTR+F+R10 -nt 6 AUTO -bb 1000 -alrt 1000*. Additionally, statistical branch supports were assessed with 1000 repetitions of UF bootstraps and SH-aLR branch tests. Trees were outgroup-rooted with *Moraxella catarrhalis* (strains BBH18 and FDAARGOS_213) and *Alkanindiges illinoisensis* DSM 15370.

SET-F: The phylogenetic tree reconstruction of SET-F followed the same general work flow as described for Set-R. However, to decrease the computational burden, trees were computed on the amino acid sequence alignments. MAFFT was run with the '--auto' parameter. Supermatrices of resulting protein MSAs were used as input for ML tree reconstruction with IQ-TREE ('-alrt 1000 -bb 1000 -nt 8 -m LG+I+G+'). Majority-rule consensus trees were computed with SplitsTree v4.14.4 [133].

Inference of hierarchical orthologous groups and reconstruction of last common ancestor dispensable and core gene sets

Hierarchical orthologous groups (HOGs) for the Set-R were inferred from the pairwise OMA orthology relations and the consensus ML species tree using the GETHOG algorithm [134] as implemented in OMA stand-alone v. 2.2.0. The Set-R pan genome was stratified by assigning each HOG to the internal node of the tree that represents the last common ancestor (LCA) of the two most distantly related taxa in the HOG. Clade-specific losses of a gene were inferred when all members of a clade lacked an ortholog that was assigned to an evolutionarily older

719 node. On this basis, we reconstructed the pan-genomes for each internal node of the tree as
720 following: We united all genes assigned to internal nodes on the path from the root to the
721 node under study and removed the union of genes that have been lost on this path.

722 ## GO annotation and GO term enrichment analysis

723 All 502,095 unique protein accessions represented in SET-R were mapped to uniprotKB
724 identifiers (UniProt accessed 9th of Febr. 2018) to obtain the annotated gene ontology (GO)
725 terms [135]. Significantly enriched GO terms were identified using a two-tailed Fischer's
726 exact test at a significance level of 0.05. Multiple test correction was done by computing the
727 false discovery rate for each term and considering only terms with an FDR < 0.05. For GO
728 term enrichment analyses at the individual internal nodes of the tree, we used the LCA pan
729 gene sets as background sets (population) and the set of genes assigned to this node as test
730 (study) set. Both sets were limited to include only genes for which orthologs are represented
731 in at least 50% of the taxa descending from this node (analysis without this cutoff is included
732 in S5 Table 3). Information about the GO terms were pulled from
733 http://purl.obolibrary.org/obo/go/go-basic.obo (accessed 22nd of June 2018). Visualization
734 of tree maps were performed with REVIGO [136].

735 ## Prediction of Secreted Proteins

736 Unless the subcellular localization of a protein was provided by uniprot, we prediceted
737 Its subcellular localization with Psortb v3.06 [137] and ngLOC v1.0 [138]. All proteins
738 classified as 'Extracellular' or 'OuterMembrane' by either tool were combined into a set of
739 secreted and accessible proteins. Conflicting predictions or cases where Psortb labeled the
740 localization of a protein as 'unknown' were resolved in favor of the ngLOC classification as it
741 demonstrated higher precision for these classes when we benchmarked both against a test-
742 set of experimentally verified proteins published by Shen et al. [139].

Annotation of Protein Function

For each protein, we considered, where available, its functional annotation provided in RefSeq, in the uniprot database, and the assigned GO terms. Additionally, we annotated the proteins with KEGG Orthology (KO) identifiers [47] using GhostKoala v2.2 [140]. Eventually, for proteins with reciprocal best blast hit orthologs in *A. baumannii* ATCC 17978, we transferred the functional annotation provided by the COG database [46] (accessed in May 21st 2020).

Virulence Factor Identification

HOGs representing known virulence factors were identified via blastp searches (v2.10.1) [141] against a custom database of virulence factors. To compile this database, we united entries of PATRIC [21] and VFDB [48] (both accessed September 23rd 2020). Subsequently, we clustered the proteins at 95% sequence similarity with cd-hit v4.6.4 [142] using the options *-G -al 0.95 -s 0.9 -c 0.95* to reduce redundancy. A HOG represents a virulence factor if any of the subsumed orthologs has a hit with >50% alignment coverage and an e-value <0.01. For all such instance the best hit's annotation was transferred.

Identification of Evolutionarily Stable Gene Clusters (ESGC)

Using the genome of *A. baumannii* ATCC 19606 as a reference, we identified clusters of consecutive genes with highly similar phyletic profiles. For this purpose, each protein-coding gene's corresponding HOG and its profile were analyzed to obtain an 8-dimensional feature vector comprised of the following values: (i-vi) clade-specific fractions of total taxa in *A. baumannii* (B), *A. calcoaceticus* (CA), *A. haemolyticus* (HA), *A. baylyi* (BA), A. *lwoffii* (LW), *A. brisouii* (BR), and *A. qingfengensis* (QI), (vii) the fraction of the total phylogenetic diversity of the ACB clade covered, and (viii) the label of the inner node the HOG was assigned to (cf. Fig 3). Four genes were excluded from the orthology search due to their short length. For these,

767 we imputed the values using the mean values of the two flanking genes. Based on these
768 vector representations, we computed a pairwise dissimilarity matrix, using the Gower
769 dissimilarity index [143]. We then arranged the genes in a graph, where a vertex between a
770 gene and its downstream neighbor was drawn, if a) their pairwise dissimilarities is smaller
771 than the 5th percentile of the gene's dissimilarity distribution across the full gene set or b) if
772 the condition *a* is met by the two genes flanking the gene. The resulting set of connected
773 components were then extracted as candidate evolutionary units.

774 ## Candidate ESGC Abundance Statistics

775 For each gene in a candidate ESGC, we computed its retention difference (RD) as the
776 difference in the fraction of taxa within the ACB clade subtracted by the fraction of taxa
777 outside the ACB clade harboring an ortholog. The candidate ESGCs were then ranked by the
778 median of the RD across all genes in the cluster. As a further measure, we devised the
779 cluster-conservation score difference (CCD), which is calculated similar to the RD score, but
780 this time assessing presence of the cluster rather than that of an individual gene. A cluster
781 was considered present only if at least 80% of its genes (orthologs) were identified and at
782 least 25% of the gene order was conserved in the genome. Here, we treated the cluster as a
783 set of ordered and oriented (considering direction of transcription) two-element tuples.
784 Clusters with a CCD below 0.25 were not further considered. For each of the resulting top
785 150 ranked clusters, we inspected cluster conservation across the taxa in Set-R and Set-F
786 using Vicinator v0.32 (https://github.com/BIONF/Vicinator). Cluster boundaries of an ESGC
787 were manually curated, when the Vicinator analysis indicated a miss due to an individually
788 bloated abundance profile (false-positive orthologs or paralogs).

Kynurenine (Kyn) cluster deletion mutant and growth experiments with *A. baumannii* Ab04

Ab04 mutant with deletion of the locus of $ESGC_{ACB}$-0452 (Ab04 Δkyn) were constructed as described previously [144]. Briefly, a FRT site-flanked apramycin resistance cassette was amplified from a variant of pKD4 [145] with primers harboring 18-25 nucleotides matching in sequence the flanking regions of the locus of $ESGC_{ACB}$-0452 (see S10 Table). Also, upstream and downstream regions of $ESGC_{ACB}$-0452 were amplified and the obtained fragments were assembled by overlap extension PCR. The PCR product was electroporated into *A. baumannii* Ab04 electrocompetent cells carrying pAT04, which expresses the RecAB recombinase induced with 2mM IPTG [1]. Mutants were selected with apramycin and integration of the resistance marker was verified by PCR. To remove the resistance cassette, electrocompetent mutants were transformed with pAT03 plasmid (which expresses the FLP recombinase) and apramycin-sensitive clones of unmarked deletion mutants were obtained. Finally, the mutant strains were confirmed by antibiotic resistance profile, PCR and genome sequencing. Ab04 WT and Ab04 Δkyn mutant strains were grown in lysogeny broth (LB) liquid medium under shaking conditions (200 rpm) at 37°C. Overnight cultures were washed three times with PBS and diluted to an OD_{600} of 0.01 in 150 µl of M9 minimal medium supplemented with 0.2% casamino acids (M9CAA), 2.5 mM L-kynurenine (Sigma, A8625) or 2.5 mM anthranilic acid (Sigma, A89855) in 96-well plates, followed by incubation at 37°C under shaking conditions in a BioTek microplate spectrophotometer. The OD_{600} values were measured every 30 min for 16h. Three independent experiments were performed with three wells per assay for each strain and condition.

Growth Experiments for Carnitine, Malate, and Glucarate

A. baumannii, A. baylyi and *A. calcoaceticus* strains were grown at 37 °C (*A. baumannii*) or 30 °C (*A. baylyi* and *A. calcoaceticus*) in mineral medium (MM) that consists of 50 mM

phosphate buffer, pH 6.8, and different salts (1 g NH_4Cl, 580 mg $MgSO_4 \times 7$ H2O, 100 mg KNO_3, 67 mg $CaCl_2 \times 2\ H_2O$, 2 mg $(NH_4)_6Mo_7O_{24} \times 4\ H_2O$, 1 ml SL9 (per liter: 12.8 g Titriplex, 2 g $FeSO_4 \times 7\ H_2O$, 190 mg $CoCl_2 \times 6\ H_2O$, 122 mg $MnCl_2 \times 4\ H_2O$, 70 mg $ZnCl_2$, 36 mg $MoNa_2O_4 \times 2\ H_2O$, 24 mg $NiCl_2 \times 6\ H_2O$, 6 mg H_3BO_3, 2 mg $CuCl_2 \times H_2O$ per l medium; pH 6.5) [146] and 20 mM of the given carbon source. Precultures were grown in MM with 20 mM Na-acetate as carbon source. Each value is the mean of +/- S.E.M. of at least three independent measurements. Growth curves were fitted manually.

821

822

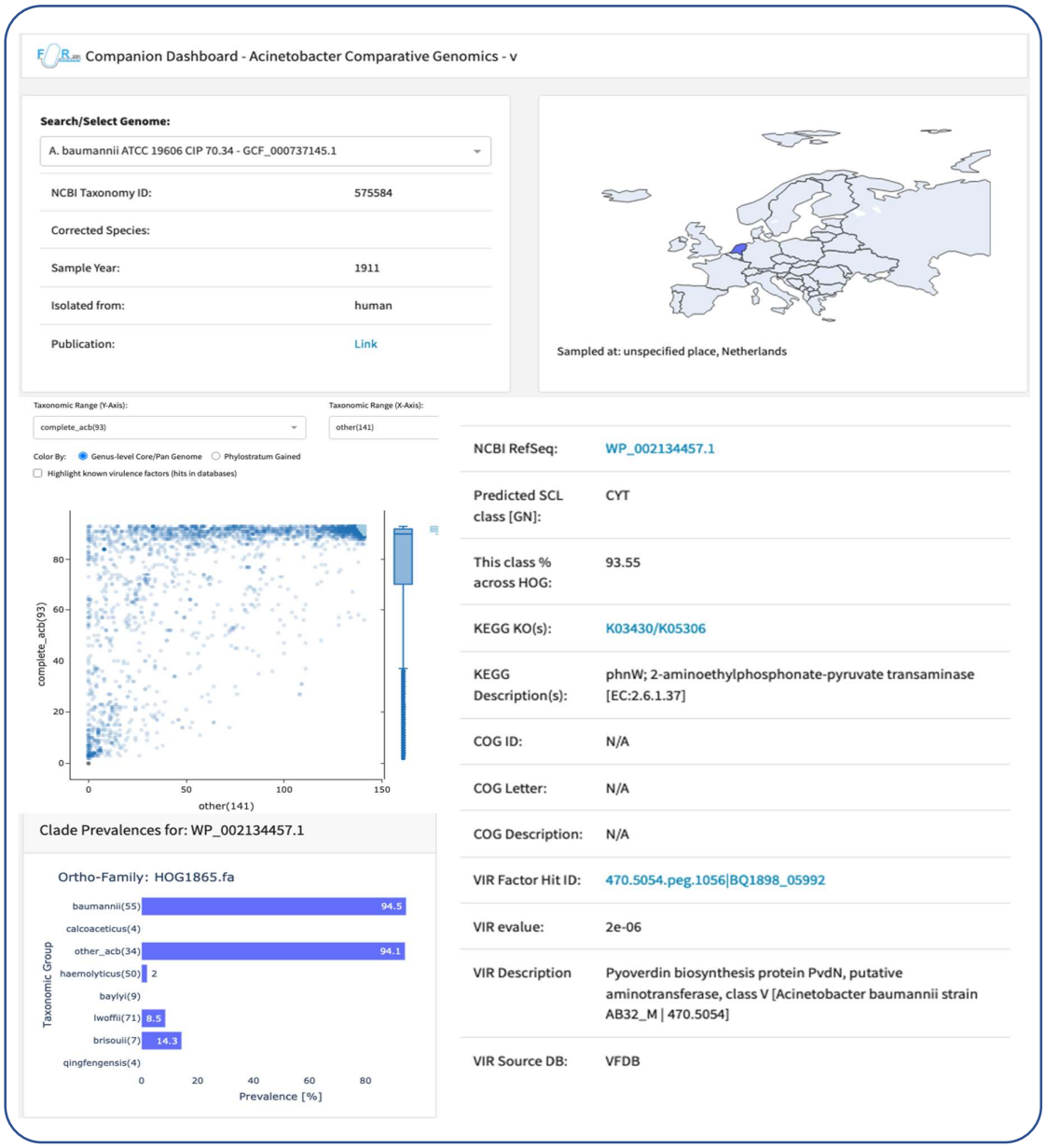

Fig 1. Aci-Dash – An interactive web-application to explore phylogenetic abundance patterns and accessory annotations for the Set-R pan-genome. *For each of the 232 strains, Aci-Dash provides further details about year and site of sampling. The interactive scatter plot reveals, for each gene of the selected strain, the abundance of orthologs in a user-defined in- and outgroup. For each gene individually, the ortholog abundance can be resolved on a clade level (cf. Fig 2), and further information including functional annotation transfer from KEGG and COG as well as known virulence factors is displayed.*

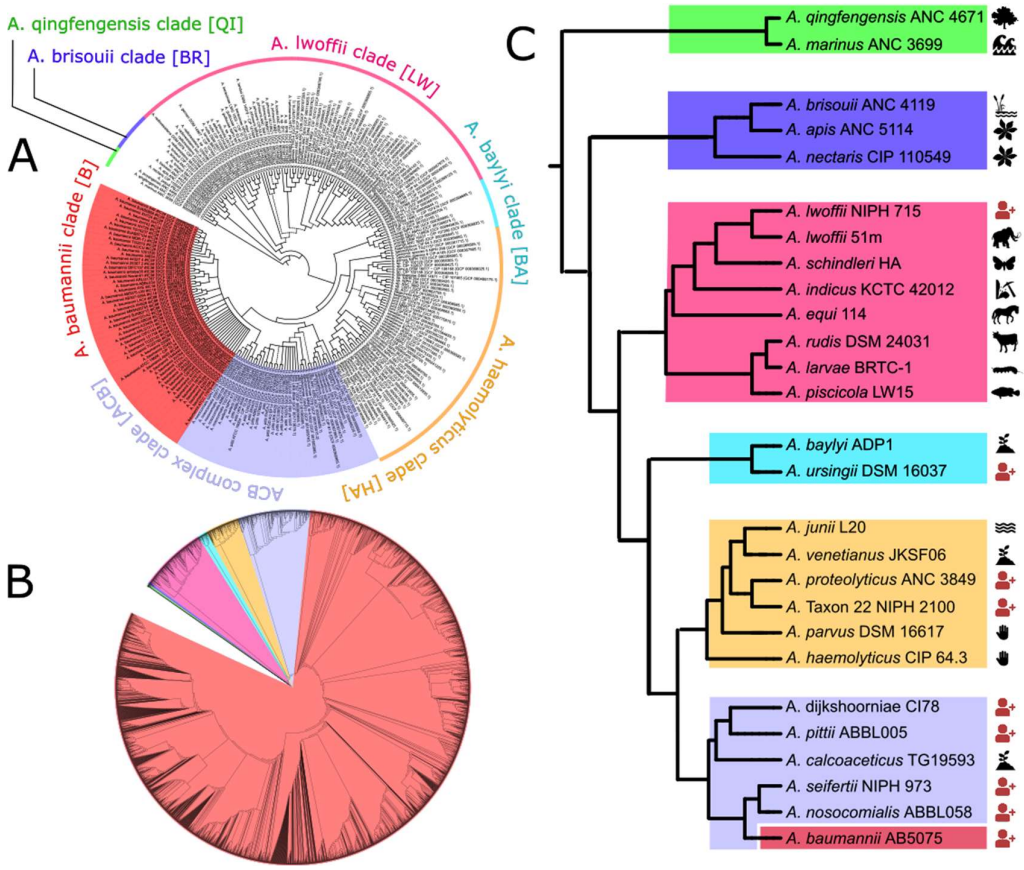

Fig 2. The phylogeny of the genus Acinetobacter. A) *Majority-rule consensus phylogeny of 232 Acinetobacter strains represented in SET-R. Solid branches are supported by all, and hatched branches by two out of three trees.* ***B)*** *The maximum likelihood tree for all 3052 taxa in Set-F. Colored clades represent the same clades as in A). A high-resolution image of this tree is provided in S8 Fig.* ***C)*** *The evolutionary backbone of the Acinetobacter genus with exemplarily chosen strains as clade representatives. The color scheme resembles that of Fig 2A. The pictograms next to the leaf labels indicate the sampling source of the particular strain. Red pictograms signal a strain that was isolated from an infected patient.*

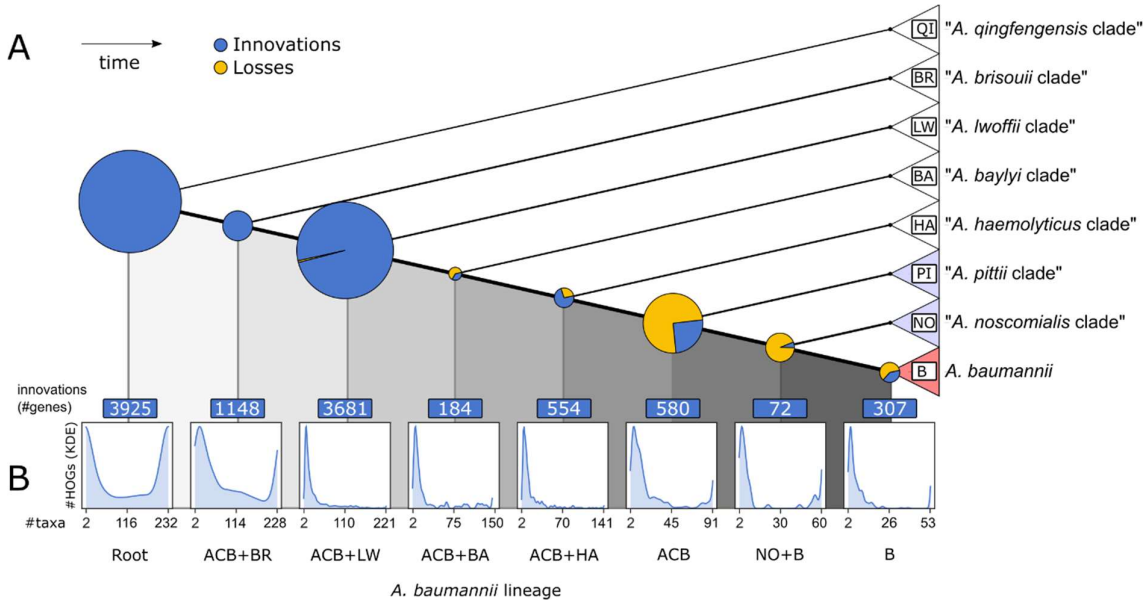

Fig 3. A phylogenetic stratification of the Acinetobacter pan-genome*. (A) Pie charts on the internal nodes indicate numbers of genes added (blue) or lost (yellow) from the respective pan-genome where the diameter is proportional to the sum of both gained and lost genes. Clades resemble those from Fig 2. (B) For each node, histograms represent the number of*

834 *descending taxa an added gene is represented in. The minimum value is 2, the maximum value is the number of taxa*
835 *subsumed in the corresponding clade.*

836

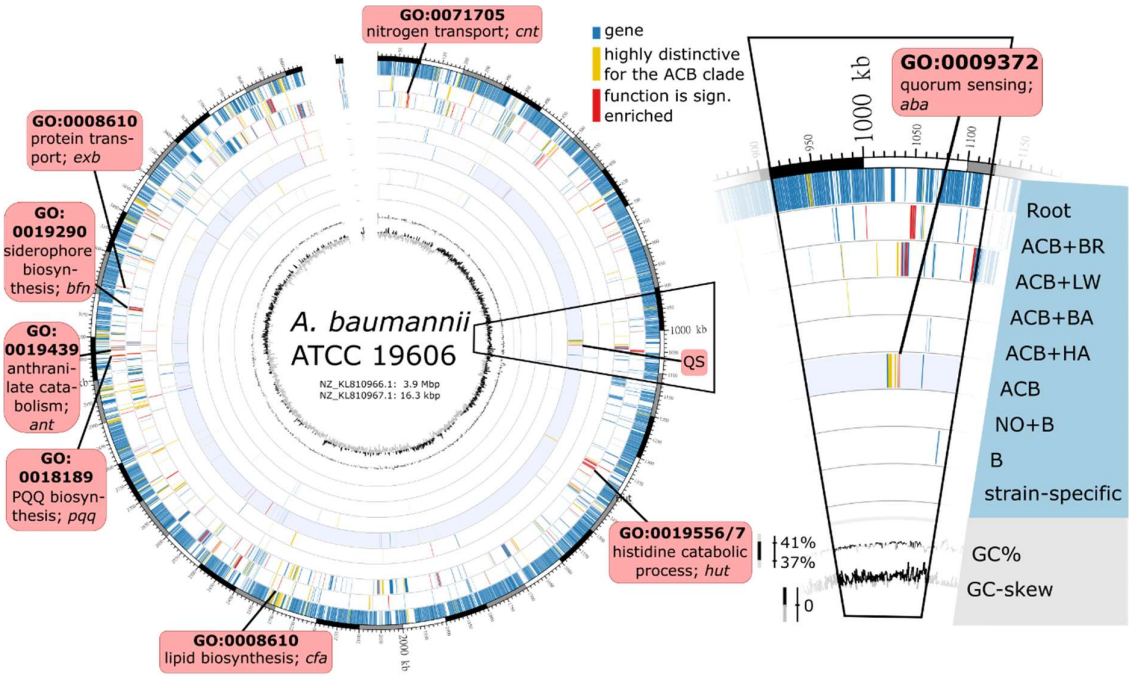

837
838 ***Fig 4. Phylogenetic strata in the protein-coding gene set of Ab. ATCC 19606.*** *Each protein-coding gene was assigned to one*
839 *of the nine layers specified in the inlay to the right (cf. Fig 3). All genes annotated with GO terms that were significantly*
840 *enriched in the individual layers are colored in red. Genes assigned to orthologous groups which were ranked within the 10*
841 *percent groups with highest retention differences (RD >=0.708, n=355) across the ATCC 19606 gene set are colored in*
842 *yellow. Red boxes highlight selected gene loci where neighboring genes contributed to the enrichment of the same GO term*
843 *(biological processes).*

844

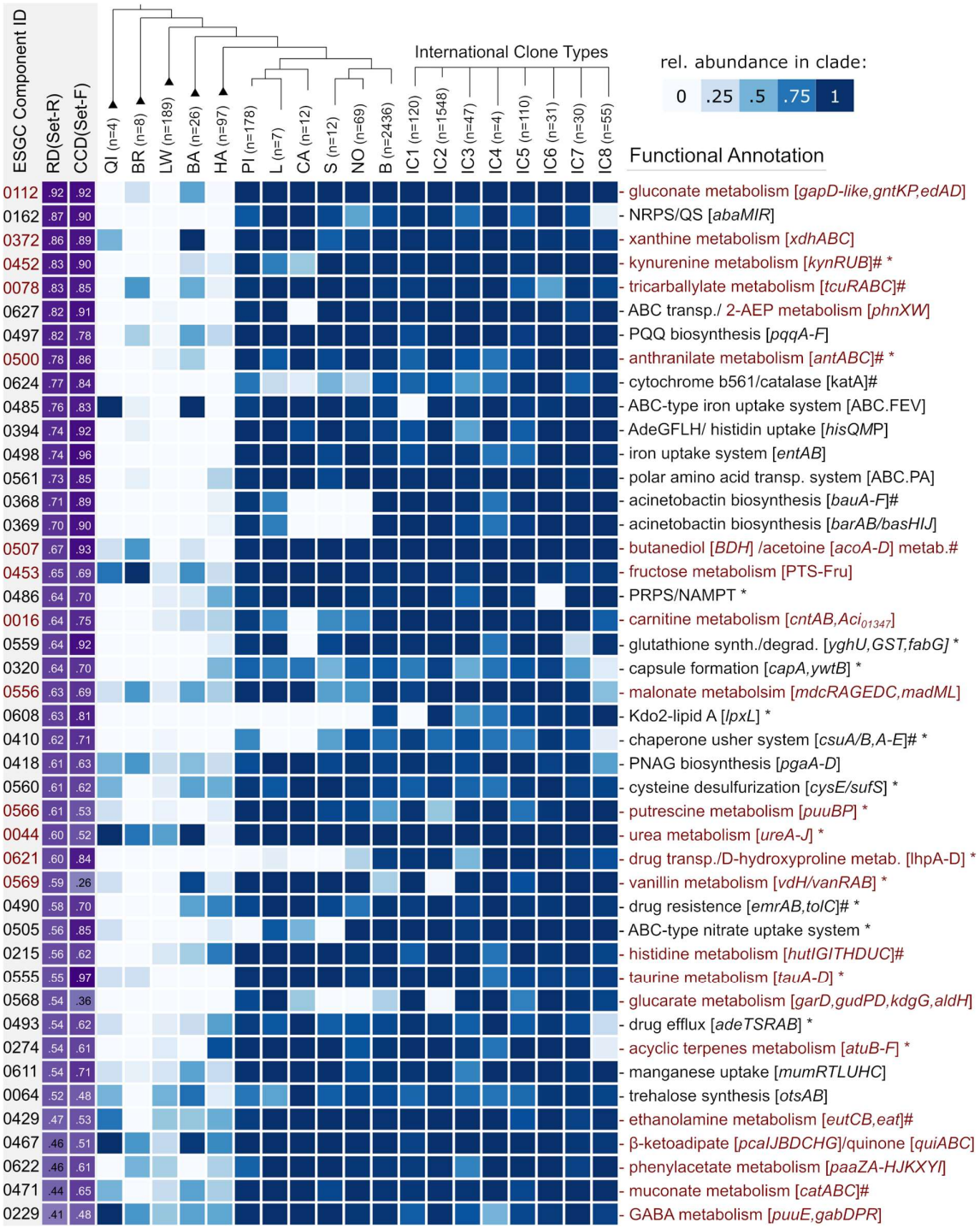

Fig 5. Phylogenetic profiles of 44 functionally annotated ESGC$_{ACB}$ across the Set-F. *Shown are the selection of ESGC$_{ACB}$ with the highest abundance difference between the ACB clade and non-ACB taxa (RD). Ids refer to the corresponding connected components provided in S6 Table 3. Gene clusters are ranked by decreasing RD. The CCD (cluster conservation difference, violet) is calculated as the difference between the relative fractions of ACB-genomes minus non-ACB genomes where the cluster is present. The heat map informs about the fraction of taxa per clade harboring the ESGC$_{ACB}$ ranging from 0 (white) to 1 (dark blue). The total number of subsumed taxa per clade are given next to the leaf label in the above tree. IC1-8 represent the cluster abundance in the 8 international clone types of A. baumannii. Clusters associated with metabolic pathways are highlighted in red. "#" marks an ESGC where we curated cluster boundaries based on literature evidence and confirmed cluster conservation using microsynteny (cf. Fig 4B). '*' marks ESGC$_{ACB}$ that encompass additional genes not covered by the functional annotation. Abbreviations: NRPS = non-ribosomal peptide synthesis; QS = quorum sensing; 2-AEP =2-aminoethylphosphonate; PNAG = polymeric ß-1,6-linked N-acetylglucosamine; NAMPT = nicotinamide phosphoribosyl transferase; PRPS = 5-phosphoribosyl pyrophosphate synthetase; GABA = gamma-aminobutyric acid; PQQ = pyrroloquinoline quinone.*

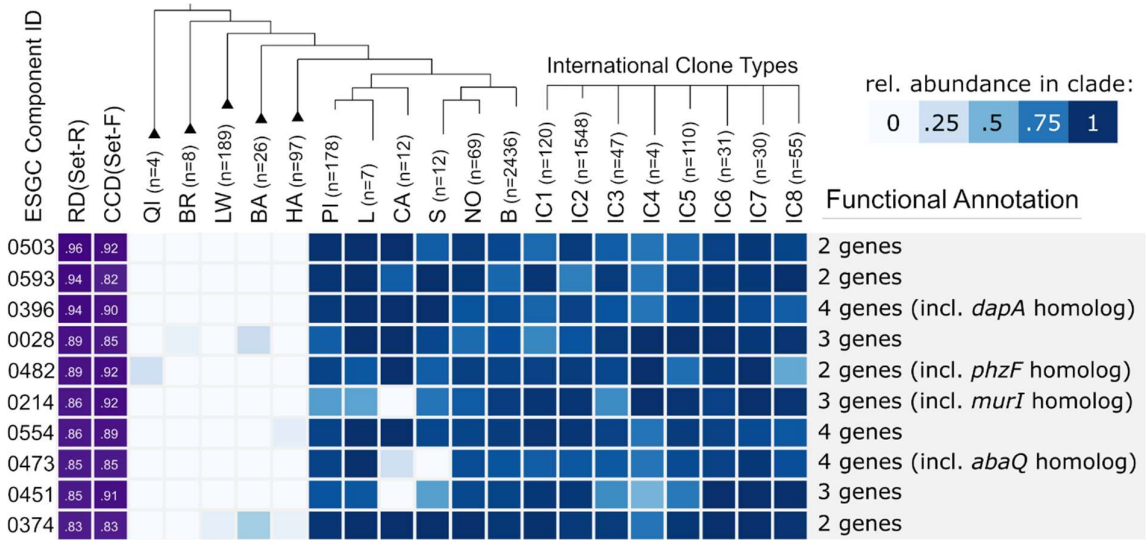

Fig 6. Top 10 ESGC$_{ACB}$ with unknown cluster function. *The genes of these clusters are mostly annotated as 'hypothetical" or "DUF-containing protein", i.e. proteins with annotated with a domain of unknown function. Due to their stable microsynteny and high prevalence across the ACB clade, they are highly interesting candidates for further functional characterization. The figure layout follows Fig 5.*

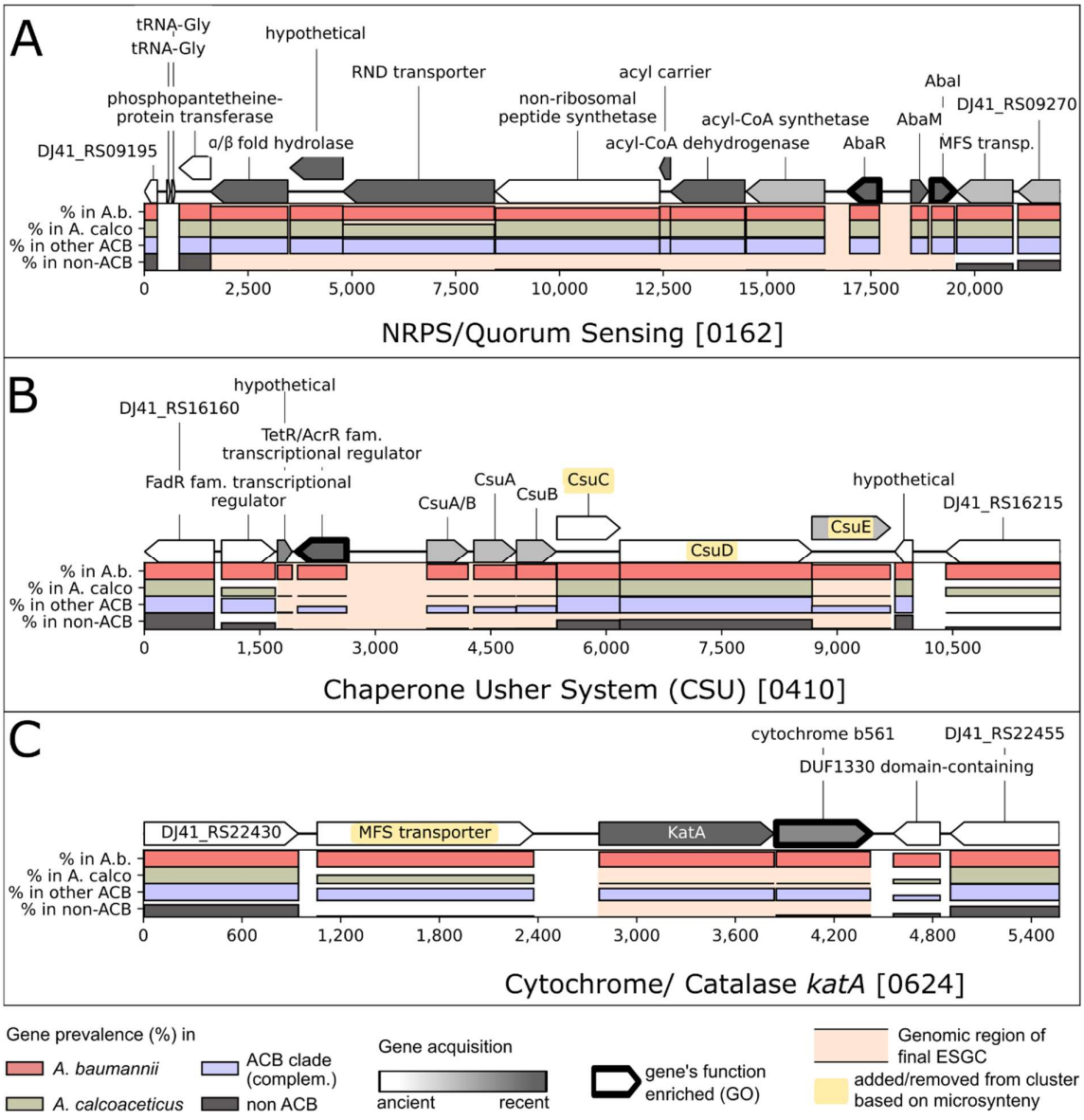

Fig 7. Three examples for $ESGC_{ACB}$ in the genome of Ab ATCC 19606. *Bar plots indicate relative abundance within the selected taxonomic groups (see legend). The $ESGC_{ACB}$ are embedded into two flanking protein-coding genes on each side that are not part of the cluster. Cluster boundaries are indicated by a pink background. Genes indicated in yellow have been either added to or excluded from the automatically generated clusters based on microsynteny analyses across Set-R. A) $ESGC_{ACB}$ – 0162 unites AbaR and AbaI (quorum sensing) with a non-ribosomal peptide synthetase cluster upstream. B) $ESGC_{ACB}$ – 0410 encompasses the cluster necessary for the Csu pilus formation. Note the deviating abundance pattern for CsuC and CsuD, which is due to the presence of prpC and prpD, two paralogous genes from the photoregulated pilus ABCD (prpABCD), in the respective orthologous groups. Microsynteny analyses confirmed that the entire Csu cluster forms one evolutionary unit (S1 Data id:0410). C) $ESGC_{ACB}$ – 0624 harbors a catalase, a cytochrome b561. Although the MFS transporter shares a similar abundance pattern across the taxa of Set-R, this transporter is not evolutionarily stably linked to the other two genes (S1 Data id:0624).*

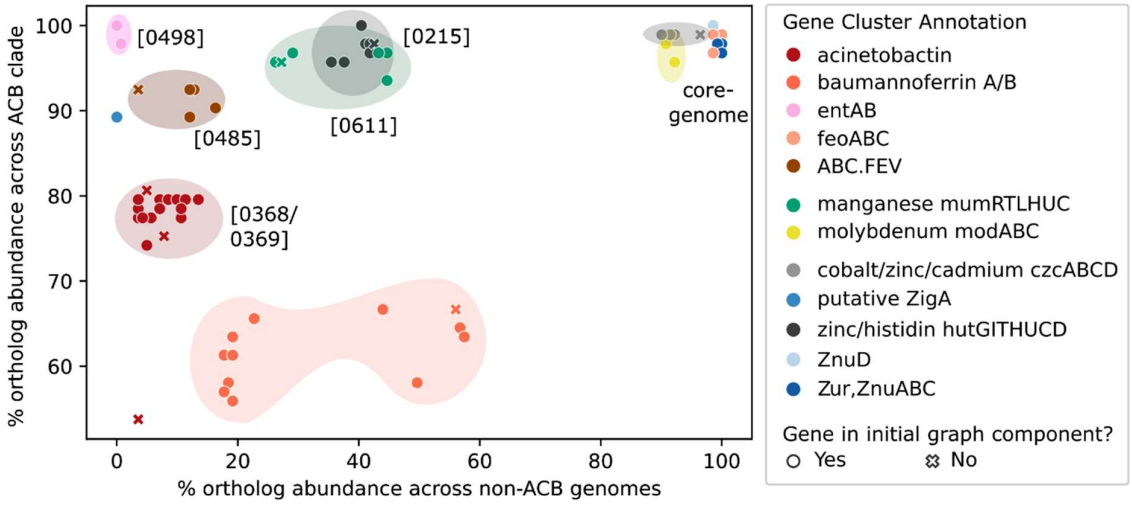

Fig 8. Abundances of micronutrient acquisition genes/clusters of Ab ATCC 19606 within and outside the ACB clade. *Absolute abundances were based on cluster-evaluation using microsynteny. Genes clusters are annotated with the $ESGC_{ACB}$ identifiers in Fig 5. Genes that are part of a cluster but missed by the initial ESGC compilation share the same color but are marked as x. Gene clusters at the top right, e.g., feoABC, represent micronutrient acquisition clusters belonging to the genus' core genome. Gene clusters at the top left, e.g., entAB, are confined to the ACB clade where they are ubiquitously present.*

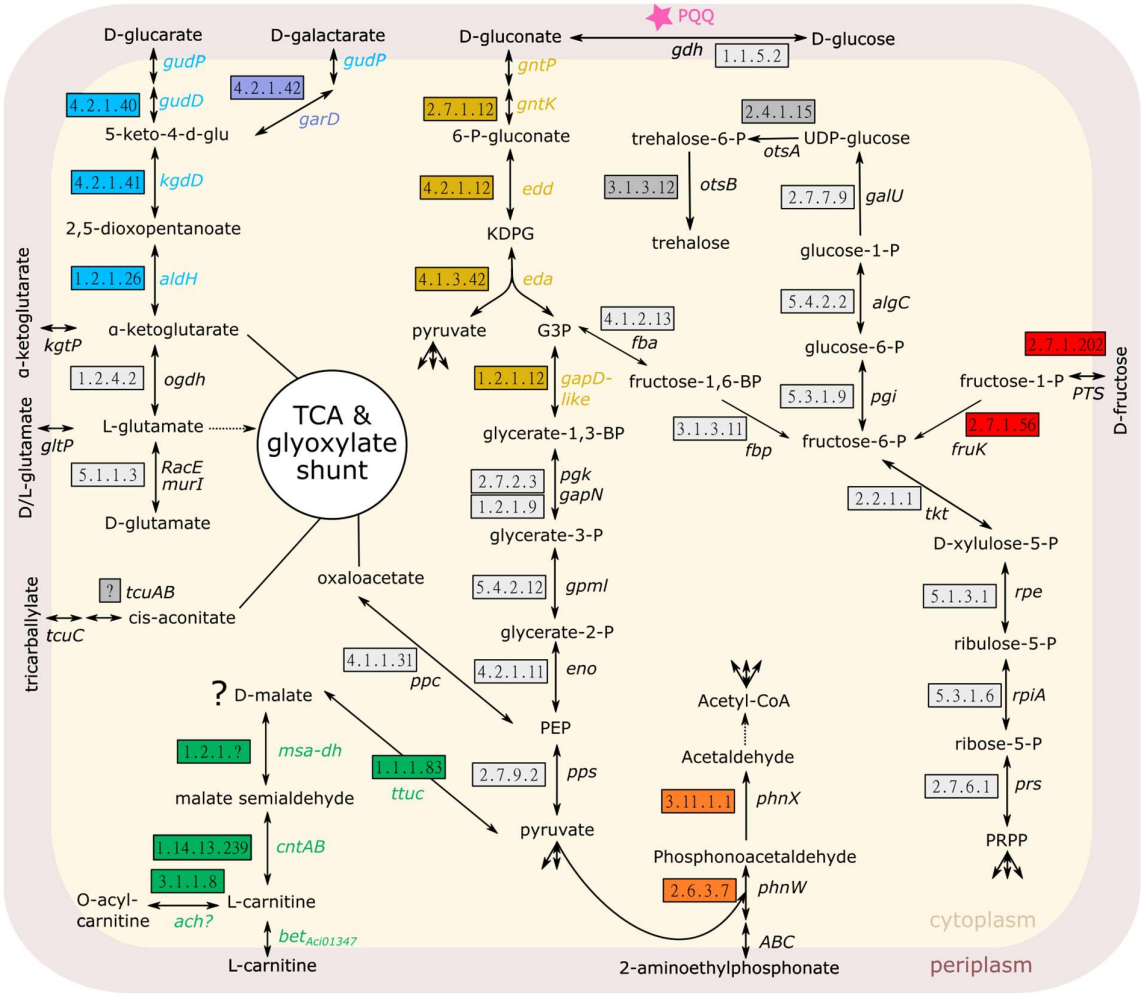

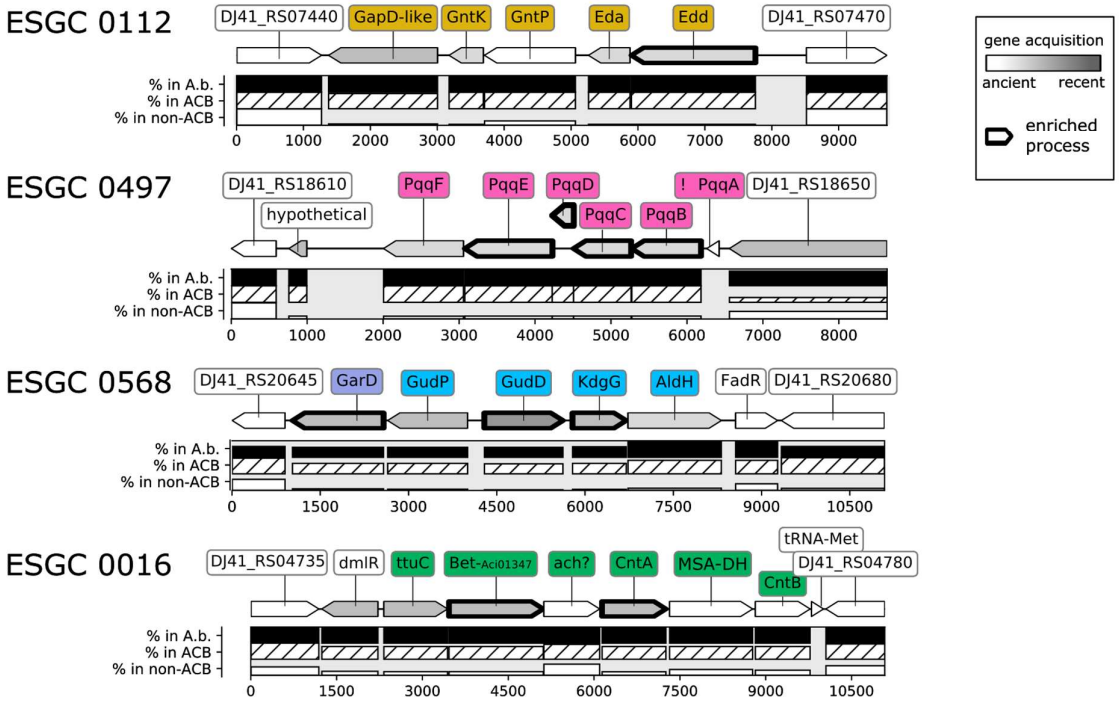

Fig 9. Members of the ACB clade have extended their basal carbohydrate metabolism. *The pathway map shows a model integrating four metabolic pathways represented by the ESGC$_{ACB}$ 0112 (Entner-Doudoroff pathway; yellow), 0497 (biosynthesis of Pyrroloquinoline quinone; magenta), 0568 (glucarate/galactarate catabolism; blue/violet) and 0016*

(carnitine catabolism; green) into the bacterial carbohydrate metabolism (grey boxes). Abbreviations: KDPG - 2-keto-3-deoxy-6-phosphogluconate; G3P – glycerinealdehyde-3-phosphate. The corresponding gene clusters are shown below the pathway map with one protein-coding flanking gene on either side that is not part of the cluster. The layout follows Fig 7. $ESGC_{ACB}$ 0112: GapD-like – glyceraldehyde-3-phosphate dehydrogenase [1.2.1.12]; GntK - gluconokinase [EC:2.7.1.12]; Edd - phosphogluconate dehydratase [EC:4.2.1.12]); Eda - 2-dehydro-3-deoxyphosphogluconate aldolase / (4S)-4-hydroxy-2-oxoglutarate aldolase [EC:4.1.2.14 4.1.3.42]; GntP - gluconate permease [E2.7.1.12]. Note, GntP shares high sequence similarity with a gluconate transporter (H+ symporter) in Escherichia coli (98% coverage, 45% identity). $ESGC_{ACB}$ 0497: pqqA-F. No abundance profile is shown for pqqA, since its length excluded it from orthology prediction (indicated by an '!'. See main text for details). $ESGC_{ACB}$ 0568: GarD - galactarate dehydratase [EC:4.2.1.42]; gudD - glucarate dehydratase [EC:4.2.1.40]; kdgD - 5-dehydro-4-deoxyglucarate dehydratase [EC:4.2.1.41]; aldH - 2,5-dioxopentanoate dehydrogenase [EC:1.2.1.26]; gudP - MFS transporter, D-glucarate/D-galactarate permease; FadR - Fatty acid metabolism regulator protein. $ESGC_{ACB}$ 0016: ttuc - D-malate dehydrogenase [EC:1.1.1.83]; Bet-Aci01347 - glycine/betaine transporter Aci01347; ach? – putative acylcarnitine hydrolase [EC:3.1.1.8]; CntAB – carnitine monooxygenase reductase subunit A and B [EC:1.14.13.239]; MSA-DH – malic semialdehyde dehydrogenase [EC:1.2.1.?]. Further colored pathways represent the clusters $ESGC_{ACB}$ 0627 (2-aminoethylphosphonate metabolism, orange), $ESGC_{ACB}$ 0453 (fructose transport/metabolism, red), $ESGC_{ACB}$ 0064 (trehalose biosynthesis, dark grey), and $ESGC_{ACB}$ 0078 tricarballylate metabolism, brown). Their corresponding genomic regions are available in S5 Fig.

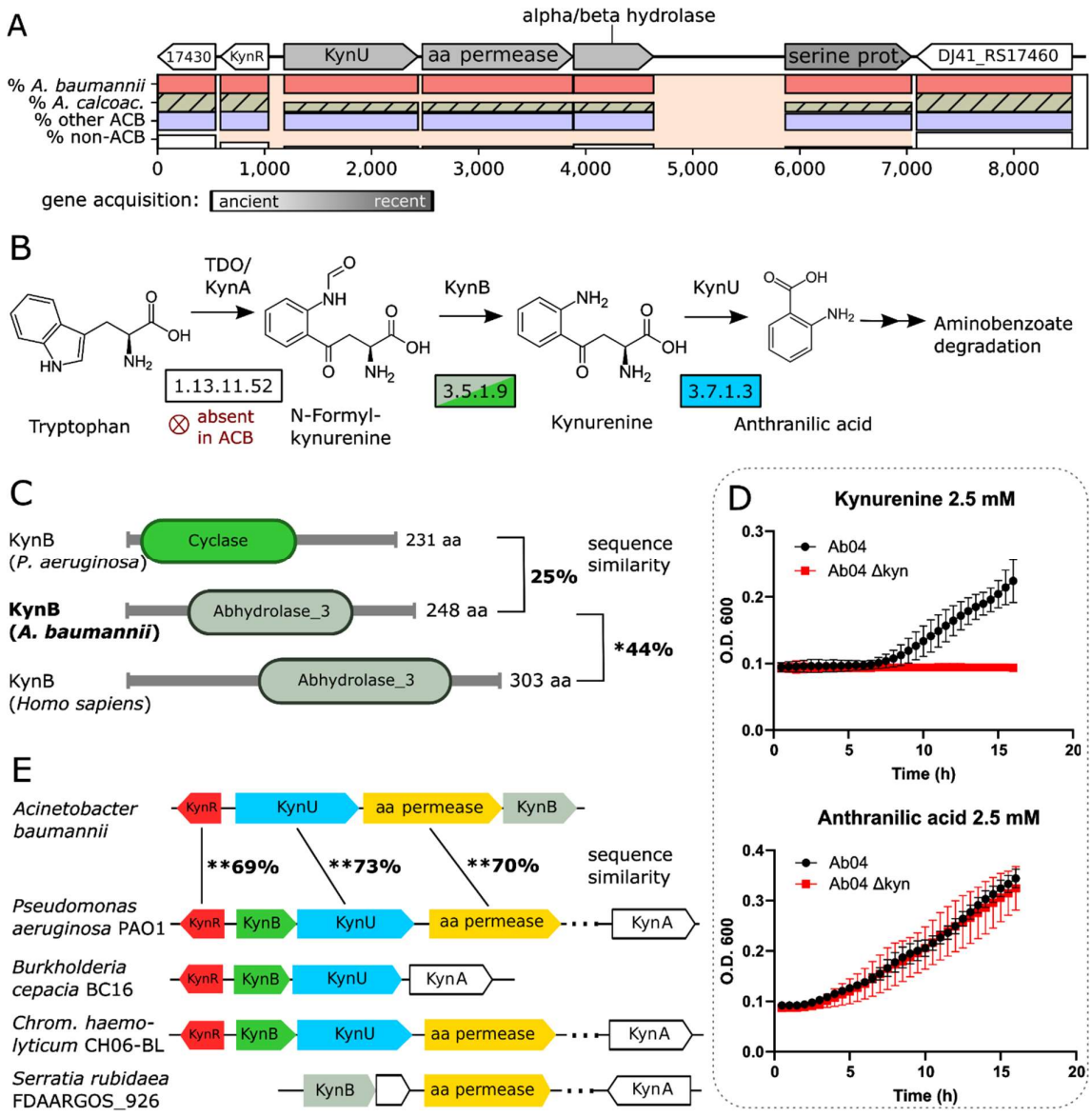

Fig 10. Evolutionary and functional characterization of the A. baumannii kynurenine pathway. *A) The locus of ESGC$_{ACB}$ 0452 in A. baumannii ATCC 19606. KynR - Lrp/AsnC family transcriptional regulator; KynU - kynurenine hydrolase; amino acid (aa) permease (uncharacterized); alpha/beta hydrolase (uncharacterized; putative kynB); serine proteinase. Cluster layout follows that of Fig 7. B) The Kynurenine pathway of tryptophan degradation. EC numbers of the enzymes catalyzing the individual reactions are given in the boxes. KynB is represented in two versions in bacteria (see C), which are represented by different colors. C) The alpha/beta hydrolase shares a significant sequence similarity and the presence of the Abhydrolase_3 Pfam domain (PF04199) with the human kynurenine formamidase (KynB or KFA) but not with KynB of P. aeruginosa, which instead harbors a Cyclase Pfam domain (PF04199) suggesting an independent evolutionary origin. D) The kynurenine cluster is necessary and sufficient for growth on kynurenine but not on anthranilic acid. Growth of Ab 04 and Ab 04 Δkyn on minimal medium supplemented with kynurenine (top) and anthranilate (bottom). E) Phylogenetic profile of the A. baumannii Kyn cluster. Numbers between the corresponding genes in Ab ATCC 19606 and PA01 represent percent sequence similarity on the amino acid level. KynB of Ab ATCC 19606 and PAO1 are not significantly similar. The Kyn cluster is shared among many proteobacterial (opportunistic) pathogens where the the Pseudomonas-type KynB is prevalent. The human-type KynB has homologs e.g., in Serratia (including S. rubideae). KynA is almost always encoded at a distant locus and entirely absent in Acinetobacter.*

Declarations

Availability of data and materials

Genomic data analyzed during the current study are publicly available in the NCBI Reference Sequence Database (RefSeq) version 87 and 204. For each selected genome, the assembly accession listed in S1 Table and S9 Table, respectively. From individual entries, we obtained genome annotation files (*.gff and *_feature_table.txt), protein sequences and coding sequences (*.faa and *cds_from_genomic.fna), and genome sequence (*_genomic.fna) files from the database [ftp://ftp.ncbi.nlm.nih.gov/refseq/release/release-catalog/archive/].
In addition, the datasets used and/or analyzed during the current study are available from the corresponding author on reasonable request.
All data generated or analyzed during this study and necessary for the interpretation are included in this published article as supplementary information.
Our custom tool Vicinator is linked (https://github.com/BIONF/Vicinator) and publicly available under the GNP license 3.0.

Competing interests

The authors declare that they have no competing interests.

Funding

This study was supported by a grant by the German Research Foundation (DFG) in the scope of the Research Group FOR2251 “Adaptation and persistence of A. baumannii.” Grant ID EB-285-2/2 to IE, AV 9/7-2 to BA, GO 2491/1-2 to SG, and WI 3272/3-2 to GW. MFF was supported by grants from the National Institute of Allergy and Infectious Diseases (grant

R01AI144120). Cloud computational resources through the de.NBI cloud are granted by the German Bundesministerium für Bildung und Forschung grant FKZ 031A533B to AG.

Authors' contribution

BD and IE conceived the study. BD performed data collection and curation, tool and app development and performed bioinformatics/statistical analyses. BD and IE together with GDV, MF, GW, BA and SG interpreted the data. SD and GDV performed and interpreted wild type and mutant strain growth experiments on kynurenine and anthranilate. JB performed growth experiments on carnitine, malate and gluconate. MAD developed the CI/CD pipeline for a containerized deployment of Aci-Dash in a cloud-platform under the supervision of AG. BD and IE drafted the manuscript, and all authors contributed to the final manuscript. All authors read and approved the final manuscript.

Acknowledgements

The authors wish to thank all researchers for making annotated genome sequences available to the public domain, Prof. Alexandr Nemec for providing on his website an accessible and up-to-date resource of the current species nomenclature of *Acinetobacter*, Vinh Tran for support with fDOG, and Ruben Iruegas for helpful discussion.

References

1. Garnacho-Montero J, Amaya-Villar R. Multiresistant Acinetobacter baumannii infections: epidemiology and management. Curr Opin Infect Dis. 2010;23(4):332-9. Epub 2010/06/29. doi: 10.1097/QCO.0b013e32833ae38b. PubMed PMID: 20581674.
2. Peleg AY, Seifert H, Paterson DL. Acinetobacter baumannii: emergence of a successful pathogen. Clin Microbiol Rev. 2008;21(3):538-82. Epub 2008/07/16. doi: 10.1128/CMR.00058-07. PubMed PMID: 18625687; PubMed Central PMCID: PMCPMC2493088.
3. Gupta N, Gandham N, Jadhav S, Mishra RN. Isolation and identification of Acinetobacter species with special reference to antibiotic resistance. J Nat Sci Biol Med.

2015;6(1):159-62. Epub 2015/03/27. doi: 10.4103/0976-9668.149116. PubMed PMID: 25810655; PubMed Central PMCID: PMCPMC4367029.

4. Sahl JW, Gillece JD, Schupp JM, Waddell VG, Driebe EM, Engelthaler DM, et al. Evolution of a pathogen: a comparative genomics analysis identifies a genetic pathway to pathogenesis in Acinetobacter. PLoS ONE. 2013;8(1):e54287. Epub 2013/02/01. doi: 10.1371/journal.pone.0054287. PubMed PMID: 23365658; PubMed Central PMCID: PMC3554770.

5. Visca P, Seifert H, Towner KJ. Acinetobacter infection--an emerging threat to human health. Iubmb Life. 2011;63(12):1048-54. Epub 2011/10/19. doi: 10.1002/iub.534. PubMed PMID: 22006724.

6. Wong D, Nielsen TB, Bonomo RA, Pantapalangkoor P, Luna B, Spellberg B. Clinical and Pathophysiological Overview of Acinetobacter Infections: a Century of Challenges. Clin Microbiol Rev. 2017;30(1):409-47. Epub 2016/12/16. doi: 10.1128/CMR.00058-16. PubMed PMID: 27974412; PubMed Central PMCID: PMCPMC5217799.

7. Weber BS, Harding CM, Feldman MF. Pathogenic Acinetobacter: from the Cell Surface to Infinity and Beyond. J Bacteriol. 2015;198(6):880-7. Epub 2015/12/30. doi: 10.1128/JB.00906-15. PubMed PMID: 26712938; PubMed Central PMCID: PMCPMC4772598.

8. Lob SH, Hoban DJ, Sahm DF, Badal RE. Regional differences and trends in antimicrobial susceptibility of Acinetobacter baumannii. Int J Antimicrob Agents. 2016;47(4):317-23. Epub 2016/03/30. doi: 10.1016/j.ijantimicag.2016.01.015. PubMed PMID: 27020541.

9. Touchon M, Cury J, Yoon EJ, Krizova L, Cerqueira GC, Murphy C, et al. The genomic diversification of the whole Acinetobacter genus: origins, mechanisms, and consequences. Genome Biol Evol. 2014;6(10):2866-82. Epub 2014/10/15. doi: 10.1093/gbe/evu225. PubMed PMID: 25313016; PubMed Central PMCID: PMCPMC4224351.

10. Giammanco A, Cala C, Fasciana T, Dowzicky MJ. Global Assessment of the Activity of Tigecycline against Multidrug-Resistant Gram-Negative Pathogens between 2004 and 2014 as Part of the Tigecycline Evaluation and Surveillance Trial. mSphere. 2017;2(1). Epub 2017/01/27. doi: 10.1128/mSphere.00310-16. PubMed PMID: 28124025; PubMed Central PMCID: PMCPMC5244261.

11. Wilharm G, Piesker J, Laue M, Skiebe E. DNA uptake by the nosocomial pathogen Acinetobacter baumannii occurs during movement along wet surfaces. J Bacteriol. 2013;195(18):4146-53. Epub 2013/07/16. doi: 10.1128/JB.00754-13. PubMed PMID: 23852865; PubMed Central PMCID: PMCPMC3754747.

12. Gallagher LA, Ramage E, Weiss EJ, Radey M, Hayden HS, Held KG, et al. Resources for Genetic and Genomic Analysis of Emerging Pathogen Acinetobacter baumannii. J Bacteriol. 2015;197(12):2027-35. Epub 2015/04/08. doi: 10.1128/JB.00131-15. PubMed PMID: 25845845; PubMed Central PMCID: PMCPMC4438207.

13. Weidensdorfer M, Ishikawa M, Hori K, Linke D, Djahanschiri B, Iruegas R, et al. The Acinetobacter trimeric autotransporter adhesin Ata controls key virulence traits of Acinetobacter baumannii. Virulence. 2019;10(1):68-81. Epub 2019/12/25. doi: 10.1080/21505594.2018.1558693. PubMed PMID: 31874074; PubMed Central PMCID: PMCPMC6363060.

14. Wieland K, Chhatwal P, Vonberg RP. Nosocomial outbreaks caused by Acinetobacter baumannii and Pseudomonas aeruginosa: Results of a systematic review. Am J Infect Control. 2018;46(6):643-8. Epub 2018/02/06. doi: 10.1016/j.ajic.2017.12.014. PubMed PMID: 29398072.

15. Lowman W, Kalk T, Menezes CN, John MA, Grobusch MP. A case of community-acquired Acinetobacter baumannii meningitis - has the threat moved beyond the hospital? J Med Microbiol. 2008;57(Pt 5):676-8. Epub 2008/04/26. doi: 10.1099/jmm.0.47781-0. PubMed PMID: 18436607.
16. Banin E, Hughes D, Kuipers OP. Editorial: Bacterial pathogens, antibiotics and antibiotic resistance. FEMS Microbiol Rev. 2017;41(3):450-2. Epub 2017/05/10. doi: 10.1093/femsre/fux016. PubMed PMID: 28486583.
17. Tacconelli E, Carrara E, Savoldi A, Harbarth S, Mendelson M, Monnet DL, et al. Discovery, research, and development of new antibiotics: the WHO priority list of antibiotic-resistant bacteria and tuberculosis. Lancet Infect Dis. 2018;18(3):318-27. Epub 2017/12/26. doi: 10.1016/S1473-3099(17)30753-3. PubMed PMID: 29276051.
18. Garcia-Quintanilla M, Pulido MR, Lopez-Rojas R, Pachon J, McConnell MJ. Emerging therapies for multidrug resistant Acinetobacter baumannii. Trends Microbiol. 2013;21(3):157-63. doi: 10.1016/j.tim.2012.12.002. PubMed PMID: 23317680.
19. Morris FC, Dexter C, Kostoulias X, Uddin MI, Peleg AY. The Mechanisms of Disease Caused by Acinetobacter baumannii. Frontiers in microbiology. 2019;10:1601. Epub 2019/08/06. doi: 10.3389/fmicb.2019.01601. PubMed PMID: 31379771; PubMed Central PMCID: PMCPMC6650576.
20. Sarshar M, Behzadi P, Scribano D, Palamara AT, Ambrosi C. Acinetobacter baumannii: An Ancient Commensal with Weapons of a Pathogen. Pathogens. 2021;10(4). Epub 2021/04/04. doi: 10.3390/pathogens10040387. PubMed PMID: 33804894; PubMed Central PMCID: PMCPMC8063835.
21. Davis JJ, Wattam AR, Aziz RK, Brettin T, Butler R, Butler RM, et al. The PATRIC Bioinformatics Resource Center: expanding data and analysis capabilities. Nucleic Acids Res. 2020;48(D1):D606-D12. Epub 2019/11/02. doi: 10.1093/nar/gkz943. PubMed PMID: 31667520; PubMed Central PMCID: PMCPMC7145515.
22. Liu B, Zheng D, Jin Q, Chen L, Yang J. VFDB 2019: a comparative pathogenomic platform with an interactive web interface. Nucleic Acids Res. 2019;47(D1):D687-D92. Epub 2018/11/06. doi: 10.1093/nar/gky1080. PubMed PMID: 30395255; PubMed Central PMCID: PMCPMC6324032.
23. Juttukonda LJ, Green ER, Lonergan ZR, Heffern MC, Chang CJ, Skaar EP. Acinetobacter baumannii OxyR Regulates the Transcriptional Response to Hydrogen Peroxide. Infect Immun. 2019;87(1). Epub 2018/10/10. doi: 10.1128/IAI.00413-18. PubMed PMID: 30297527; PubMed Central PMCID: PMCPMC6300632.
24. McConnell MJ, Actis L, Pachon J. Acinetobacter baumannii: human infections, factors contributing to pathogenesis and animal models. FEMS Microbiol Rev. 2013;37(2):130-55. Epub 2012/05/10. doi: 10.1111/j.1574-6976.2012.00344.x. PubMed PMID: 22568581.
25. Harding CM, Hennon SW, Feldman MF. Uncovering the mechanisms of Acinetobacter baumannii virulence. Nat Rev Microbiol. 2018;16(2):91-102. Epub 2017/12/19. doi: 10.1038/nrmicro.2017.148. PubMed PMID: 29249812; PubMed Central PMCID: PMCPMC6571207.
26. Giles SK, Stroeher UH, Eijkelkamp BA, Brown MH. Identification of genes essential for pellicle formation in Acinetobacter baumannii. BMC Microbiol. 2015;15:116. Epub 2015/06/07. doi: 10.1186/s12866-015-0440-6. PubMed PMID: 26047954; PubMed Central PMCID: PMCPMC4457973.
27. Green ER, Juttukonda LJ, Skaar EP. The Manganese-Responsive Transcriptional Regulator MumR Protects Acinetobacter baumannii from Oxidative Stress. Infect Immun.

2020;88(3). Epub 2019/12/04. doi: 10.1128/IAI.00762-19. PubMed PMID: 31792075; PubMed Central PMCID: PMCPMC7035938.

28. Ramirez MS, Penwell WF, Traglia GM, Zimbler DL, Gaddy JA, Nikolaidis N, et al. Identification of Potential Virulence Factors in the Model Strain Acinetobacter baumannii A118. Frontiers in microbiology. 2019;10:1599. Epub 2019/08/10. doi: 10.3389/fmicb.2019.01599. PubMed PMID: 31396168; PubMed Central PMCID: PMCPMC6663985.

29. Eisenreich W, Dandekar T, Heesemann J, Goebel W. Carbon metabolism of intracellular bacterial pathogens and possible links to virulence. Nat Rev Microbiol. 2010;8(6):401-12. Epub 2010/05/11. doi: 10.1038/nrmicro2351. PubMed PMID: 20453875.

30. Passalacqua KD, Charbonneau ME, O'Riordan MXD. Bacterial Metabolism Shapes the Host-Pathogen Interface. Microbiol Spectr. 2016;4(3). Epub 2016/06/24. doi: 10.1128/microbiolspec.VMBF-0027-2015. PubMed PMID: 27337445; PubMed Central PMCID: PMCPMC4922512.

31. Nemec A. Classification and nomenclature of species in the genus Acinetobacter 2020. Available from: https://apps.szu.cz/anemec/Classification.pdf.

32. Al Atrouni A, Joly-Guillou ML, Hamze M, Kempf M. Reservoirs of Non-baumannii Acinetobacter Species. Front Microbiol. 2016;7:49. Epub 2016/02/13. doi: 10.3389/fmicb.2016.00049. PubMed PMID: 26870013; PubMed Central PMCID: PMCPMC4740782.

33. Wallace L, Daugherty SC, Nagaraj S, Johnson JK, Harris AD, Rasko DA. Use of Comparative Genomics To Characterize the Diversity of Acinetobacter baumannii Surveillance Isolates in a Health Care Institution. Antimicrob Agents Chemother. 2016;60(10):5933-41. Epub 2016/07/28. doi: 10.1128/AAC.00477-16. PubMed PMID: 27458211; PubMed Central PMCID: PMCPMC5038335.

34. Holt K, Kenyon JJ, Hamidian M, Schultz MB, Pickard DJ, Dougan G, et al. Five decades of genome evolution in the globally distributed, extensively antibiotic-resistant Acinetobacter baumannii global clone 1. Microb Genom. 2016;2(2):e000052. Epub 2017/03/30. doi: 10.1099/mgen.0.000052. PubMed PMID: 28348844; PubMed Central PMCID: PMCPMC5320584.

35. Chan AP, Sutton G, DePew J, Krishnakumar R, Choi Y, Huang XZ, et al. A novel method of consensus pan-chromosome assembly and large-scale comparative analysis reveal the highly flexible pan-genome of Acinetobacter baumannii. Genome Biol. 2015;16:143. Epub 2015/07/22. doi: 10.1186/s13059-015-0701-6. PubMed PMID: 26195261; PubMed Central PMCID: PMCPMC4507327.

36. Imperi F, Antunes LCS, Blom J, Villa L, Iacono M, Visca P, et al. The Genomics of Acinetobacter baumannii: Insights into Genome Plasticity, Antimicrobial Resistance and Pathogenicity. Iubmb Life. 2011;63(12):1068-74. doi: Doi 10.1002/Iub.531. PubMed PMID: ISI:000297947900005.

37. Abbott I, Cerqueira GM, Bhuiyan S, Peleg AY. Carbapenem resistance in Acinetobacter baumannii: laboratory challenges, mechanistic insights and therapeutic strategies. Expert Rev Anti Infect Ther. 2013;11(4):395-409. Epub 2013/04/10. doi: 10.1586/eri.13.21. PubMed PMID: 23566149.

38. Eijkelkamp BA, Stroeher UH, Hassan KA, Paulsen IT, Brown MH. Comparative analysis of surface-exposed virulence factors of Acinetobacter baumannii. BMC Genomics. 2014;15:1020. Epub 2014/11/26. doi: 10.1186/1471-2164-15-1020. PubMed PMID: 25422040; PubMed Central PMCID: PMCPMC4256060.

39. Antunes LC, Visca P, Towner KJ. Acinetobacter baumannii: evolution of a global pathogen. Pathog Dis. 2014;71(3):292-301. Epub 2014/01/01. doi: 10.1111/2049-632X.12125. PubMed PMID: 24376225.
40. Peleg AY, de Breij A, Adams MD, Cerqueira GM, Mocali S, Galardini M, et al. The success of acinetobacter species; genetic, metabolic and virulence attributes. PLoS ONE. 2012;7(10):e46984. Epub 2012/11/13. doi: 10.1371/journal.pone.0046984. PubMed PMID: 23144699; PubMed Central PMCID: PMC3483291.
41. Meumann EM, Anstey NM, Currie BJ, Piera KA, Kenyon JJ, Hall RM, et al. Genomic epidemiology of severe community-onset Acinetobacter baumannii infection. Microb Genom. 2019;5(3). Epub 2019/02/27. doi: 10.1099/mgen.0.000258. PubMed PMID: 30806611; PubMed Central PMCID: PMCPMC6487312.
42. O'Leary NA, Wright MW, Brister JR, Ciufo S, Haddad D, McVeigh R, et al. Reference sequence (RefSeq) database at NCBI: current status, taxonomic expansion, and functional annotation. Nucleic Acids Res. 2016;44(D1):D733-45. Epub 2015/11/11. doi: 10.1093/nar/gkv1189. PubMed PMID: 26553804; PubMed Central PMCID: PMCPMC4702849.
43. Comai S, Bertazzo A, Brughera M, Crotti S. Chapter Five - Tryptophan in health and disease. In: Makowski GS, editor. Advances in Clinical Chemistry. 95: Elsevier; 2020. p. 165-218.
44. Costantini C, Bellet MM, Renga G, Stincardini C, Borghi M, Pariano M, et al. Tryptophan Co-Metabolism at the Host-Pathogen Interface. Front Immunol. 2020;11:67. Epub 2020/02/23. doi: 10.3389/fimmu.2020.00067. PubMed PMID: 32082324; PubMed Central PMCID: PMCPMC7001157.
45. Altenhoff AM, Levy J, Zarowiecki M, Tomiczek B, Warwick Vesztrocy A, Dalquen DA, et al. OMA standalone: orthology inference among public and custom genomes and transcriptomes. Genome Res. 2019;29(7):1152-63. Epub 2019/06/27. doi: 10.1101/gr.243212.118. PubMed PMID: 31235654; PubMed Central PMCID: PMCPMC6633268.
46. Galperin MY, Kristensen DM, Makarova KS, Wolf YI, Koonin EV. Microbial genome analysis: the COG approach. Brief Bioinform. 2019;20(4):1063-70. Epub 2017/10/03. doi: 10.1093/bib/bbx117. PubMed PMID: 28968633; PubMed Central PMCID: PMCPMC6781585.
47. Kanehisa M, Sato Y, Kawashima M, Furumichi M, Tanabe M. KEGG as a reference resource for gene and protein annotation. Nucleic Acids Res. 2016;44(D1):D457-62. doi: 10.1093/nar/gkv1070. PubMed PMID: 26476454; PubMed Central PMCID: PMCPMC4702792.
48. Chen L, Yang J, Yu J, Yao Z, Sun L, Shen Y, et al. VFDB: a reference database for bacterial virulence factors. Nucleic Acids Res. 2005;33(Database issue):D325-8. Epub 2004/12/21. doi: 10.1093/nar/gki008. PubMed PMID: 15608208; PubMed Central PMCID: PMCPMC539962.
49. Snitkin ES, Zelazny AM, Montero CI, Stock F, Mijares L, Murray PR, et al. Genome-wide recombination drives diversification of epidemic strains of Acinetobacter baumannii. Proc Natl Acad Sci U S A. 2011;108(33):13758-63. doi: 10.1073/pnas.1104404108.
50. Mirarab S, Warnow T. ASTRAL-II: coalescent-based species tree estimation with many hundreds of taxa and thousands of genes. Bioinformatics. 2015;31(12):i44-52. Epub 2015/06/15. doi: 10.1093/bioinformatics/btv234. PubMed PMID: 26072508; PubMed Central PMCID: PMCPMC4765870.
51. Mateo-Estrada V, Grana-Miraglia L, Lopez-Leal G, Castillo-Ramirez S. Phylogenomics Reveals Clear Cases of Misclassification and Genus-Wide Phylogenetic Markers for

Acinetobacter. Genome Biol Evol. 2019;11(9):2531-41. Epub 2019/08/14. doi: 10.1093/gbe/evz178. PubMed PMID: 31406982; PubMed Central PMCID: PMCPMC6740150.

52. Qin J, Feng Y, Lu X, Zong Z. Precise Species Identification for Acinetobacter: a Genome-Based Study with Description of Two Novel Acinetobacter Species. mSystems. 2021;6(3):e0023721. Epub 2021/06/02. doi: 10.1128/mSystems.00237-21. PubMed PMID: 34061620; PubMed Central PMCID: PMCPMC8269215.

53. Kim PS, Shin NR, Kim JY, Yun JH, Hyun DW, Bae JW. Acinetobacter apis sp. nov., isolated from the intestinal tract of a honey bee, Apis mellifera. J Microbiol. 2014;52(8):639-45. Epub 2014/08/08. doi: 10.1007/s12275-014-4078-0. PubMed PMID: 25098562.

54. Ellegaard KM, Engel P. Genomic diversity landscape of the honey bee gut microbiota. Nature communications. 2019;10(1):446. Epub 2019/01/27. doi: 10.1038/s41467-019-08303-0. PubMed PMID: 30683856; PubMed Central PMCID: PMCPMC6347622.

55. McFrederick QS, Rehan SM. Characterization of pollen and bacterial community composition in brood provisions of a small carpenter bee. Molecular ecology. 2016;25(10):2302-11. Epub 2016/03/08. doi: 10.1111/mec.13608. PubMed PMID: 26945527.

56. Karah N, Haldorsen B, Hegstad K, Simonsen GS, Sundsfjord A, Samuelsen O, et al. Species identification and molecular characterization of Acinetobacter spp. blood culture isolates from Norway. The Journal of antimicrobial chemotherapy. 2011;66(4):738-44. Epub 2011/03/12. doi: 10.1093/jac/dkq521. PubMed PMID: 21393175.

57. Turton JF, Shah J, Ozongwu C, Pike R. Incidence of Acinetobacter species other than A. baumannii among clinical isolates of Acinetobacter: evidence for emerging species. J Clin Microbiol. 2010;48(4):1445-9. Epub 2010/02/26. doi: 10.1128/JCM.02467-09. PubMed PMID: 20181894; PubMed Central PMCID: PMCPMC2849580.

58. Niu C, Clemmer KM, Bonomo RA, Rather PN. Isolation and characterization of an autoinducer synthase from Acinetobacter baumannii. J Bacteriol. 2008;190(9):3386-92. Epub 2008/02/19. doi: 10.1128/JB.01929-07. PubMed PMID: 18281398; PubMed Central PMCID: PMCPMC2347373.

59. Bhargava N, Sharma P, Capalash N. Quorum sensing in Acinetobacter: an emerging pathogen. Crit Rev Microbiol. 2010;36(4):349-60. Epub 2010/09/18. doi: 10.3109/1040841X.2010.512269. PubMed PMID: 20846031.

60. Clemmer KM, Bonomo RA, Rather PN. Genetic analysis of surface motility in Acinetobacter baumannii. Microbiology. 2011;157(Pt 9):2534-44. Epub 2011/06/28. doi: 10.1099/mic.0.049791-0. PubMed PMID: 21700662; PubMed Central PMCID: PMCPMC3352170.

61. Choudhary KS, Hudaiberdiev S, Gelencser Z, Goncalves Coutinho B, Venturi V, Pongor S. The organization of the quorum sensing luxI/R family genes in Burkholderia. Int J Mol Sci. 2013;14(7):13727-47. Epub 2013/07/04. doi: 10.3390/ijms140713727. PubMed PMID: 23820583; PubMed Central PMCID: PMCPMC3742214.

62. Le Guillouzer S, Groleau MC, Deziel E. Two rsaM Homologues Encode Central Regulatory Elements Modulating Quorum Sensing in Burkholderia thailandensis. J Bacteriol. 2018;200(14). Epub 2018/03/07. doi: 10.1128/JB.00727-17. PubMed PMID: 29507087; PubMed Central PMCID: PMCPMC6018367.

63. Lopez-Martin M, Dubern JF, Alexander MR, Williams P. AbaM Regulates Quorum Sensing, Biofilm Formation, and Virulence in Acinetobacter baumannii. J Bacteriol. 2021;203(8). Epub 2021/01/27. doi: 10.1128/JB.00635-20. PubMed PMID: 33495249; PubMed Central PMCID: PMCPMC8088503.

64. Rumbo-Feal S, Gomez MJ, Gayoso C, Alvarez-Fraga L, Cabral MP, Aransay AM, et al. Whole transcriptome analysis of Acinetobacter baumannii assessed by RNA-sequencing

reveals different mRNA expression profiles in biofilm compared to planktonic cells. PLoS One. 2013;8(8):e72968. Epub 2013/09/12. doi: 10.1371/journal.pone.0072968. PubMed PMID: 24023660; PubMed Central PMCID: PMCPMC3758355.

65. Rumbo-Feal S, Perez A, Ramelot TA, Alvarez-Fraga L, Vallejo JA, Beceiro A, et al. Contribution of the A. baumannii A1S_0114 Gene to the Interaction with Eukaryotic Cells and Virulence. Front Cell Infect Microbiol. 2017;7:108. Epub 2017/04/20. doi: 10.3389/fcimb.2017.00108. PubMed PMID: 28421168; PubMed Central PMCID: PMCPMC5376624.

66. Puri AW, Schaefer AL, Fu Y, Beck DAC, Greenberg EP, Lidstrom ME. Quorum Sensing in a Methane-Oxidizing Bacterium. J Bacteriol. 2017;199(5). Epub 2016/12/21. doi: 10.1128/JB.00773-16. PubMed PMID: 27994019; PubMed Central PMCID: PMCPMC5309911.

67. Gonzalez O, Ortiz-Castro R, Diaz-Perez C, Diaz-Perez AL, Magana-Duenas V, Lopez-Bucio J, et al. Non-ribosomal Peptide Synthases from Pseudomonas aeruginosa Play a Role in Cyclodipeptide Biosynthesis, Quorum-Sensing Regulation, and Root Development in a Plant Host. Microb Ecol. 2017;73(3):616-29. Epub 2016/12/03. doi: 10.1007/s00248-016-0896-4. PubMed PMID: 27900439.

68. Tomaras AP, Dorsey CW, Edelmann RE, Actis LA. Attachment to and biofilm formation on abiotic surfaces by Acinetobacter baumannii: involvement of a novel chaperone-usher pili assembly system. Microbiology. 2003;149(Pt 12):3473-84. Epub 2003/12/10. doi: 10.1099/mic.0.26541-0. PubMed PMID: 14663080.

69. Pakharukova N, Tuittila M, Paavilainen S, Malmi H, Parilova O, Teneberg S, et al. Structural basis for Acinetobacter baumannii biofilm formation. Proc Natl Acad Sci U S A. 2018;115(21):5558-63. Epub 2018/05/08. doi: 10.1073/pnas.1800961115. PubMed PMID: 29735695; PubMed Central PMCID: PMCPMC6003481.

70. Colclough AL, Scadden J, Blair JMA. TetR-family transcription factors in Gram-negative bacteria: conservation, variation and implications for efflux-mediated antimicrobial resistance. BMC Genomics. 2019;20(1):731. Epub 2019/10/14. doi: 10.1186/s12864-019-6075-5. PubMed PMID: 31606035; PubMed Central PMCID: PMCPMC6790063.

71. Cuthbertson L, Nodwell JR. The TetR family of regulators. Microbiol Mol Biol Rev. 2013;77(3):440-75. Epub 2013/09/06. doi: 10.1128/MMBR.00018-13. PubMed PMID: 24006471; PubMed Central PMCID: PMCPMC3811609.

72. Tomaras AP, Flagler MJ, Dorsey CW, Gaddy JA, Actis LA. Characterization of a two-component regulatory system from Acinetobacter baumannii that controls biofilm formation and cellular morphology. Microbiology. 2008;154(Pt 11):3398-409. Epub 2008/10/30. doi: 10.1099/mic.0.2008/019471-0. PubMed PMID: 18957593.

73. Cerqueira GM, Kostoulias X, Khoo C, Aibinu I, Qu Y, Traven A, et al. A global virulence regulator in Acinetobacter baumannii and its control of the phenylacetic acid catabolic pathway. J Infect Dis. 2014;210(1):46-55. Epub 2014/01/17. doi: 10.1093/infdis/jiu024. PubMed PMID: 24431277.

74. Sun D, Crowell SA, Harding CM, De Silva PM, Harrison A, Fernando DM, et al. KatG and KatE confer Acinetobacter resistance to hydrogen peroxide but sensitize bacteria to killing by phagocytic respiratory burst. Life Sci. 2016;148:31-40. Epub 2016/02/11. doi: 10.1016/j.lfs.2016.02.015. PubMed PMID: 26860891; PubMed Central PMCID: PMCPMC4792659.

75. Slauch JM. How does the oxidative burst of macrophages kill bacteria? Still an open question. Mol Microbiol. 2011;80(3):580-3. Epub 2011/03/08. doi: 10.1111/j.1365-2958.2011.07612.x. PubMed PMID: 21375590; PubMed Central PMCID: PMCPMC3109634.

76. Nguyen GT, Green ER, Mecsas J. Neutrophils to the ROScue: Mechanisms of NADPH Oxidase Activation and Bacterial Resistance. Front Cell Infect Microbiol. 2017;7:373. Epub 2017/09/12. doi: 10.3389/fcimb.2017.00373. PubMed PMID: 28890882; PubMed Central PMCID: PMCPMC5574878.
77. Mortensen BL, Skaar EP. The contribution of nutrient metal acquisition and metabolism to Acinetobacter baumannii survival within the host. Front Cell Infect Microbiol. 2013;3:95. Epub 2014/01/01. doi: 10.3389/fcimb.2013.00095. PubMed PMID: 24377089; PubMed Central PMCID: PMCPMC3859900.
78. Eijkelkamp BA, Hassan KA, Paulsen IT, Brown MH. Investigation of the human pathogen Acinetobacter baumannii under iron limiting conditions. BMC Genomics. 2011;12:126. Epub 2011/02/24. doi: 10.1186/1471-2164-12-126. PubMed PMID: 21342532; PubMed Central PMCID: PMCPMC3055841.
79. El-Zaatari M, Chang YM, Zhang M, Franz M, Shreiner A, McDermott AJ, et al. Tryptophan catabolism restricts IFN-gamma-expressing neutrophils and Clostridium difficile immunopathology. J Immunol. 2014;193(2):807-16. Epub 2014/06/18. doi: 10.4049/jimmunol.1302913. PubMed PMID: 24935925; PubMed Central PMCID: PMCPMC4091639.
80. Sheldon JR, Skaar EP. Acinetobacter baumannii can use multiple siderophores for iron acquisition, but only acinetobactin is required for virulence. PLoS Pathog. 2020;16(10):e1008995. Epub 2020/10/20. doi: 10.1371/journal.ppat.1008995. PubMed PMID: 33075115; PubMed Central PMCID: PMCPMC7595644 following competing interests: Dr. Eric Skaar served as a consultant to Shionogi Inc.
81. Nairn BL, Lonergan ZR, Wang J, Braymer JJ, Zhang Y, Calcutt MW, et al. The Response of Acinetobacter baumannii to Zinc Starvation. Cell Host Microbe. 2016;19(6):826-36. Epub 2016/06/10. doi: 10.1016/j.chom.2016.05.007. PubMed PMID: 27281572; PubMed Central PMCID: PMCPMC4901392.
82. Jakubovics NS, Jenkinson HF. Out of the iron age: new insights into the critical role of manganese homeostasis in bacteria. Microbiology (Reading). 2001;147(Pt 7):1709-18. Epub 2001/06/29. doi: 10.1099/00221287-147-7-1709. PubMed PMID: 11429449.
83. Anjem A, Varghese S, Imlay JA. Manganese import is a key element of the OxyR response to hydrogen peroxide in Escherichia coli. Mol Microbiol. 2009;72(4):844-58. Epub 2009/04/30. doi: 10.1111/j.1365-2958.2009.06699.x. PubMed PMID: 19400769; PubMed Central PMCID: PMCPMC2776087.
84. Juttukonda LJ, Chazin WJ, Skaar EP. Acinetobacter baumannii Coordinates Urea Metabolism with Metal Import To Resist Host-Mediated Metal Limitation. mBio. 2016;7(5). Epub 2016/09/30. doi: 10.1128/mBio.01475-16. PubMed PMID: 27677795; PubMed Central PMCID: PMCPMC5050338.
85. Krizova L, Maixnerova M, Sedo O, Nemec A. Acinetobacter albensis sp. nov., isolated from natural soil and water ecosystems. Int J Syst Evol Microbiol. 2015;65(11):3905-12. Epub 2015/08/08. doi: 10.1099/ijsem.0.000511. PubMed PMID: 26245775.
86. Zhao J, Zhu Y, Han J, Lin YW, Aichem M, Wang J, et al. Genome-Scale Metabolic Modeling Reveals Metabolic Alterations of Multidrug-Resistant Acinetobacter baumannii in a Murine Bloodstream Infection Model. Microorganisms. 2020;8(11). Epub 2020/11/20. doi: 10.3390/microorganisms8111793. PubMed PMID: 33207684; PubMed Central PMCID: PMCPMC7696501.
87. Zhu Y, Zhao J, Maifiah MHM, Velkov T, Schreiber F, Li J. Metabolic Responses to Polymyxin Treatment in Acinetobacter baumannii ATCC 19606: Integrating Transcriptomics and Metabolomics with Genome-Scale Metabolic Modeling. mSystems. 2019;4(1). Epub

2019/02/13. doi: 10.1128/mSystems.00157-18. PubMed PMID: 30746493; PubMed Central PMCID: PMCPMC6365644.

88. Farrugia DN, Elbourne LD, Hassan KA, Eijkelkamp BA, Tetu SG, Brown MH, et al. The complete genome and phenome of a community-acquired Acinetobacter baumannii. PLoS One. 2013;8(3):e58628. Epub 2013/03/26. doi: 10.1371/journal.pone.0058628. PubMed PMID: 23527001; PubMed Central PMCID: PMCPMC3602452.

89. Durot M, Le Fevre F, de Berardinis V, Kreimeyer A, Vallenet D, Combe C, et al. Iterative reconstruction of a global metabolic model of Acinetobacter baylyi ADP1 using high-throughput growth phenotype and gene essentiality data. BMC Syst Biol. 2008;2:85. Epub 2008/10/09. doi: 10.1186/1752-0509-2-85. PubMed PMID: 18840283; PubMed Central PMCID: PMCPMC2606687.

90. Nemec A. Metabolic and physiological characteristics of Acinetobacter species 2021. Available from: https://apps.szu.cz/anemec/Phenotype.pdf.

91. Matsushita K, Toyama H, Ameyama M, Adachi O, Dewanti A, Duine JA. Soluble and Membrane-bound Quinoprotein D-Glucose Dehydrogenases of the Acinetobacter calcoaceticus: The Binding Process of PQQ to the Apoenzymes. Bioscience, Biotechnology, and Biochemistry. 1995;59(8):1548-55. doi: 10.1271/bbb.59.1548.

92. Shen YQ, Bonnot F, Imsand EM, RoseFigura JM, Sjolander K, Klinman JP. Distribution and properties of the genes encoding the biosynthesis of the bacterial cofactor, pyrroloquinoline quinone. Biochemistry. 2012;51(11):2265-75. Epub 2012/02/14. doi: 10.1021/bi201763d. PubMed PMID: 22324760; PubMed Central PMCID: PMCPMC3334298.

93. Riquelme SA, Ahn D, Prince A. Pseudomonas aeruginosa and Klebsiella pneumoniae Adaptation to Innate Immune Clearance Mechanisms in the Lung. J Innate Immun. 2018;10(5-6):442-54. Epub 2018/04/05. doi: 10.1159/000487515. PubMed PMID: 29617698; PubMed Central PMCID: PMCPMC6785651.

94. Nemec A. 2021.

95. Blumenthal HJ, Lucuta VL, Blumenthal DC. Specific enzymatic assay for D-glucarate in human serum. Anal Biochem. 1990;185(2):286-93. Epub 1990/03/01. doi: 10.1016/0003-2697(90)90294-j. PubMed PMID: 2187374.

96. Lamichhane-Khadka R, Benoit SL, Maier SE, Maier RJ. A link between gut community metabolism and pathogenesis: molecular hydrogen-stimulated glucarate catabolism aids Salmonella virulence. Open Biol. 2013;3(12):130146. Epub 2013/12/07. doi: 10.1098/rsob.130146. PubMed PMID: 24307595; PubMed Central PMCID: PMCPMC3877842.

97. Rosas-Lemus M, Minasov G, Shuvalova L, Wawrzak Z, Kiryukhina O, Mih N, et al. Structure of galactarate dehydratase, a new fold in an enolase involved in bacterial fitness after antibiotic treatment. Protein Sci. 2020;29(3):711-22. Epub 2019/12/08. doi: 10.1002/pro.3796. PubMed PMID: 31811683; PubMed Central PMCID: PMCPMC7021002.

98. Reuter SE, Evans AM. Carnitine and acylcarnitines: pharmacokinetic, pharmacological and clinical aspects. Clin Pharmacokinet. 2012;51(9):553-72. Epub 2012/07/19. doi: 10.2165/11633940-000000000-00000
10.1007/BF03261931. PubMed PMID: 22804748.

99. Zhu Y, Jameson E, Crosatti M, Schafer H, Rajakumar K, Bugg TD, et al. Carnitine metabolism to trimethylamine by an unusual Rieske-type oxygenase from human microbiota. Proc Natl Acad Sci U S A. 2014;111(11):4268-73. Epub 2014/03/05. doi: 10.1073/pnas.1316569111. PubMed PMID: 24591617; PubMed Central PMCID: PMCPMC3964110.

100. Bouvet PJM, Grimont PAD. Taxonomy of the Genus Acinetobacter with the Recognition of Acinetobacter baumannii sp. nov., Acinetobacter haemolyticus sp. nov., Acinetobacter johnsonii sp. nov., and Acinetobacter junii sp. nov. and Emended Descriptions of Acinetobacter calcoaceticus and Acinetobacter lwoffii. International Journal of Systematic and Evolutionary Microbiology. 1986;36(2):228-40. doi: https://doi.org/10.1099/00207713-36-2-228.

101. Breisch J, Waclawska I, Averhoff B. Identification and characterization of a carnitine transporter in Acinetobacter baumannii. Microbiologyopen. 2019;8(6):e00752. Epub 2018/10/16. doi: 10.1002/mbo3.752. PubMed PMID: 30318737; PubMed Central PMCID: PMCPMC6562126.

102. Wang CH, Zhao TX, Li M, Zhang C, Xing XH. Characterization of a novel Acinetobacter baumannii xanthine dehydrogenase expressed in Escherichia coli. Biotechnol Lett. 2016;38(2):337-44. Epub 2015/11/07. doi: 10.1007/s10529-015-1986-y. PubMed PMID: 26543035.

103. Altenhoff AM, Glover NM, Train CM, Kaleb K, Warwick Vesztrocy A, Dylus D, et al. The OMA orthology database in 2018: retrieving evolutionary relationships among all domains of life through richer web and programmatic interfaces. Nucleic Acids Res. 2018;46(D1):D477-D85. Epub 2017/11/07. doi: 10.1093/nar/gkx1019. PubMed PMID: 29106550; PubMed Central PMCID: PMCPMC5753216.

104. Knoten CA, Hudson LL, Coleman JP, Farrow JM, 3rd, Pesci EC. KynR, a Lrp/AsnC-type transcriptional regulator, directly controls the kynurenine pathway in Pseudomonas aeruginosa. J Bacteriol. 2011;193(23):6567-75. Epub 2011/10/04. doi: 10.1128/JB.05803-11. PubMed PMID: 21965577; PubMed Central PMCID: PMCPMC3232868.

105. Bortolotti P, Hennart B, Thieffry C, Jausions G, Faure E, Grandjean T, et al. Tryptophan catabolism in Pseudomonas aeruginosa and potential for inter-kingdom relationship. BMC Microbiol. 2016;16(1):137. Epub 2016/07/09. doi: 10.1186/s12866-016-0756-x. PubMed PMID: 27392067; PubMed Central PMCID: PMCPMC4938989.

106. Rohmer L, Hocquet D, Miller SI. Are pathogenic bacteria just looking for food? Metabolism and microbial pathogenesis. Trends Microbiol. 2011;19(7):341-8. Epub 2011/05/24. doi: 10.1016/j.tim.2011.04.003. PubMed PMID: 21600774; PubMed Central PMCID: PMCPMC3130110.

107. Fournier P-E, Vallenet D, Barbe V, Audic S, Ogata H, Poirel L, et al. Comparative Genomics of Multidrug Resistance in Acinetobacter baumannii. PLoS Genet. 2006;2(1):e7. doi: 10.1371/journal.pgen.0020007.

108. Sato Y, Unno Y, Miyazaki C, Ubagai T, Ono Y. Multidrug-resistant Acinetobacter baumannii resists reactive oxygen species and survives in macrophages. Sci Rep. 2019;9(1):17462. Epub 2019/11/27. doi: 10.1038/s41598-019-53846-3. PubMed PMID: 31767923; PubMed Central PMCID: PMCPMC6877552.

109. Chen YJ, Leung PM, Wood JL, Bay SK, Hugenholtz P, Kessler AJ, et al. Metabolic flexibility allows bacterial habitat generalists to become dominant in a frequently disturbed ecosystem. ISME J. 2021. Epub 2021/05/05. doi: 10.1038/s41396-021-00988-w. PubMed PMID: 33941890.

110. Ren W, Rajendran R, Zhao Y, Tan B, Wu G, Bazer FW, et al. Amino Acids As Mediators of Metabolic Cross Talk between Host and Pathogen. Front Immunol. 2018;9:319. Epub 2018/03/15. doi: 10.3389/fimmu.2018.00319. PubMed PMID: 29535717; PubMed Central PMCID: PMCPMC5835074.

111. Chen Y, Guillemin GJ. Kynurenine pathway metabolites in humans: disease and healthy States. Int J Tryptophan Res. 2009;2:1-19. Epub 2009/01/01. doi: 10.4137/ijtr.s2097. PubMed PMID: 22084578; PubMed Central PMCID: PMCPMC3195227.
112. Genestet C, Le Gouellec A, Chaker H, Polack B, Guery B, Toussaint B, et al. Scavenging of reactive oxygen species by tryptophan metabolites helps Pseudomonas aeruginosa escape neutrophil killing. Free Radic Biol Med. 2014;73:400-10. Epub 2014/06/15. doi: 10.1016/j.freeradbiomed.2014.06.003. PubMed PMID: 24929180.
113. Page AJ, Taylor B, Keane JA. Multilocus sequence typing by blast from de novo assemblies against PubMLST. Journal of Open Source Software. 2016;1(8):118. doi: 10.21105/joss.00118.
114. Bartual SG, Seifert H, Hippler C, Luzon MA, Wisplinghoff H, Rodriguez-Valera F. Development of a multilocus sequence typing scheme for characterization of clinical isolates of Acinetobacter baumannii. J Clin Microbiol. 2005;43(9):4382-90. Epub 2005/09/08. doi: 10.1128/JCM.43.9.4382-4390.2005. PubMed PMID: 16145081; PubMed Central PMCID: PMCPMC1234098.
115. Diancourt L, Passet V, Nemec A, Dijkshoorn L, Brisse S. The population structure of Acinetobacter baumannii: expanding multiresistant clones from an ancestral susceptible genetic pool. PLoS One. 2010;5(4):e10034. Epub 2010/04/13. doi: 10.1371/journal.pone.0010034. PubMed PMID: 20383326; PubMed Central PMCID: PMCPMC2850921.
116. Wang X, Qiao F, Yu R, Gao Y, Zong Z. Clonal diversity of Acinetobacter baumannii clinical isolates revealed by a snapshot study. BMC Microbiol. 2013;13:234. Epub 2013/10/23. doi: 10.1186/1471-2180-13-234. PubMed PMID: 24144168; PubMed Central PMCID: PMCPMC3815251.
117. Wilharm G, Skiebe E, Higgins PG, Poppel MT, Blaschke U, Leser S, et al. Relatedness of wildlife and livestock avian isolates of the nosocomial pathogen Acinetobacter baumannii to lineages spread in hospitals worldwide. Environ Microbiol. 2017;19(10):4349-64. Epub 2017/09/20. doi: 10.1111/1462-2920.13931. PubMed PMID: 28925528.
118. Cerezales M, Xanthopoulou K, Wille J, Bustamante Z, Seifert H, Gallego L, et al. Acinetobacter baumannii analysis by core genome multi-locus sequence typing in two hospitals in Bolivia: endemicity of international clone 7 isolates (CC25). Int J Antimicrob Agents. 2019;53(6):844-9. Epub 2019/04/01. doi: 10.1016/j.ijantimicag.2019.03.019. PubMed PMID: 30928684.
119. Kumar S, Patil PP, Singhal L, Ray P, Patil PB, Gautam V. Molecular epidemiology of carbapenem-resistant Acinetobacter baumannii isolates reveals the emergence of blaOXA-23 and blaNDM-1 encoding international clones in India. Infect Genet Evol. 2019;75:103986. Epub 2019/07/31. doi: 10.1016/j.meegid.2019.103986. PubMed PMID: 31362071.
120. Higgins PG, Hrenovic J, Seifert H, Dekic S. Characterization of Acinetobacter baumannii from water and sludge line of secondary wastewater treatment plant. Water Res. 2018;140:261-7. Epub 2018/05/04. doi: 10.1016/j.watres.2018.04.057. PubMed PMID: 29723815.
121. Levy-Blitchtein S, Roca I, Plasencia-Rebata S, Vicente-Taboada W, Velasquez-Pomar J, Munoz L, et al. Emergence and spread of carbapenem-resistant Acinetobacter baumannii international clones II and III in Lima, Peru. Emerg Microbes Infect. 2018;7(1):119. Epub 2018/07/05. doi: 10.1038/s41426-018-0127-9. PubMed PMID: 29970918; PubMed Central PMCID: PMCPMC6030224.
122. Tomaschek F, Higgins PG, Stefanik D, Wisplinghoff H, Seifert H. Head-to-Head Comparison of Two Multi-Locus Sequence Typing (MLST) Schemes for Characterization of

Acinetobacter baumannii Outbreak and Sporadic Isolates. PLoS One. 2016;11(4):e0153014. Epub 2016/04/14. doi: 10.1371/journal.pone.0153014. PubMed PMID: 27071077; PubMed Central PMCID: PMCPMC4829225.

123. Higgins PG, Prior K, Harmsen D, Seifert H. Development and evaluation of a core genome multilocus typing scheme for whole-genome sequence-based typing of Acinetobacter baumannii. PLoS One. 2017;12(6):e0179228. Epub 2017/06/09. doi: 10.1371/journal.pone.0179228. PubMed PMID: 28594944; PubMed Central PMCID: PMCPMC5464626.

124. Gaiarsa S, Batisti Biffignandi G, Esposito EP, Castelli M, Jolley KA, Brisse S, et al. Comparative Analysis of the Two Acinetobacter baumannii Multilocus Sequence Typing (MLST) Schemes. Frontiers in microbiology. 2019;10:930. Epub 2019/05/28. doi: 10.3389/fmicb.2019.00930. PubMed PMID: 31130931; PubMed Central PMCID: PMCPMC6510311.

125. Chernomor O, Minh BQ, Forest F, Klaere S, Ingram T, Henzinger M, et al. Split diversity in constrained conservation prioritization using integer linear programming. Methods Ecol Evol. 2015;6(1):83-91. Epub 2015/04/22. doi: 10.1111/2041-210X.12299. PubMed PMID: 25893087; PubMed Central PMCID: PMCPMC4392707.

126. Kurtz S, Phillippy A, Delcher AL, Smoot M, Shumway M, Antonescu C, et al. Versatile and open software for comparing large genomes. Genome Biol. 2004;5(2):R12. Epub 2004/02/05. doi: 10.1186/gb-2004-5-2-r12. PubMed PMID: 14759262; PubMed Central PMCID: PMCPMC395750.

127. Pritchard L, Glover RH, Humphris S, Elphinstone JG, Toth IK. Genomics and taxonomy in diagnostics for food security: soft-rotting enterobacterial plant pathogens. Analytical Methods. 2016;8(1):12-24. doi: 10.1039/C5AY02550H.

128. Birikmen M, Bohnsack KE, Tran V, Somayaji S, Bohnsack MT, Ebersberger I. Tracing Eukaryotic Ribosome Biogenesis Factors Into the Archaeal Domain Sheds Light on the Evolution of Functional Complexity. Frontiers in microbiology. 2021;12:2598.

129. Tettelin H, Masignani V, Cieslewicz MJ, Donati C, Medini D, Ward NL, et al. Genome analysis of multiple pathogenic isolates of Streptococcus agalactiae: implications for the microbial "pan-genome". Proc Natl Acad Sci U S A. 2005;102(39):13950-5. Epub 2005/09/21. doi: 10.1073/pnas.0506758102. PubMed PMID: 16172379; PubMed Central PMCID: PMCPMC1216834.

130. Katoh K, Toh H. Recent Developments in the MAFFT Multiple Sequence Alignment Program. Brief Bioinform. 2008;9(4):286-98.

131. Suyama M, Torrents D, Bork P. PAL2NAL: robust conversion of protein sequence alignments into the corresponding codon alignments. Nucleic Acids Res. 2006;34(Web Server issue):W609-12. Epub 2006/07/18. doi: 10.1093/nar/gkl315. PubMed PMID: 16845082; PubMed Central PMCID: PMCPMC1538804.

132. Nguyen LT, Schmidt HA, von Haeseler A, Minh BQ. IQ-TREE: a fast and effective stochastic algorithm for estimating maximum-likelihood phylogenies. Mol Biol Evol. 2015;32(1):268-74. doi: 10.1093/molbev/msu300. PubMed PMID: 25371430; PubMed Central PMCID: PMCPMC4271533.

133. Huson DH. SplitsTree: analyzing and visualizing evolutionary data. Bioinformatics. 1998;14(1):68-73. PubMed PMID: 9520503.

134. Altenhoff AM, Gil M, Gonnet GH, Dessimoz C. Inferring hierarchical orthologous groups from orthologous gene pairs. PLoS One. 2013;8(1):e53786. Epub 2013/01/24. doi: 10.1371/journal.pone.0053786. PubMed PMID: 23342000; PubMed Central PMCID: PMCPMC3544860.

135. The Gene Ontology C. The Gene Ontology Resource: 20 years and still GOing strong. Nucleic Acids Res. 2019;47(D1):D330-D8. Epub 2018/11/06. doi: 10.1093/nar/gky1055. PubMed PMID: 30395331; PubMed Central PMCID: PMCPMC6323945.
136. Supek F, Bošnjak M, Škunca N, Šmuc T. REVIGO Summarizes and Visualizes Long Lists of Gene Ontology Terms. PLOS ONE. 2011;6(7):e21800. doi: 10.1371/journal.pone.0021800.
137. Yu NY, Wagner JR, Laird MR, Melli G, Rey S, Lo R, et al. PSORTb 3.0: improved protein subcellular localization prediction with refined localization subcategories and predictive capabilities for all prokaryotes. Bioinformatics. 2010;26(13):1608-15. Epub 2010/05/18. doi: 10.1093/bioinformatics/btq249. PubMed PMID: 20472543; PubMed Central PMCID: PMCPMC2887053.
138. King BR, Vural S, Pandey S, Barteau A, Guda C. ngLOC: software and web server for predicting protein subcellular localization in prokaryotes and eukaryotes. BMC research notes. 2012;5:351. Epub 2012/07/12. doi: 10.1186/1756-0500-5-351. PubMed PMID: 22780965; PubMed Central PMCID: PMCPMC3532370.
139. Shen HB, Chou KC. Gneg-mPLoc: a top-down strategy to enhance the quality of predicting subcellular localization of Gram-negative bacterial proteins. J Theor Biol. 2010;264(2):326-33. Epub 2010/01/23. doi: 10.1016/j.jtbi.2010.01.018. PubMed PMID: 20093124.
140. Kanehisa M, Sato Y, Morishima K. BlastKOALA and GhostKOALA: KEGG Tools for Functional Characterization of Genome and Metagenome Sequences. J Mol Biol. 2016;428(4):726-31. doi: 10.1016/j.jmb.2015.11.006. PubMed PMID: 26585406.
141. Altschul SF, Madden TL, Schäffer AA, Zhang J, Zhang Z, Miller W, et al. Gapped BLAST and PSI-BLAST: a new generation of protein database search programs. Nucleic Acids Res. 1997;25(17):3389-402.
142. Fu L, Niu B, Zhu Z, Wu S, Li W. CD-HIT: accelerated for clustering the next-generation sequencing data. Bioinformatics. 2012;28(23):3150-2. Epub 2012/10/13. doi: 10.1093/bioinformatics/bts565. PubMed PMID: 23060610; PubMed Central PMCID: PMCPMC3516142.
143. Gower JC, Warrens MJ. Similarity, Dissimilarity, and Distance, Measures of. Wiley StatsRef: Statistics Reference Online. Hoboken, New Jersey, US: John Wiley & Sons, Ltd.; 2014.
144. Tucker AT, Nowicki EM, Boll JM, Knauf GA, Burdis NC, Trent MS, et al. Defining gene-phenotype relationships in Acinetobacter baumannii through one-step chromosomal gene inactivation. mBio. 2014;5(4):e01313-14. Epub 2014/08/07. doi: 10.1128/mBio.01313-14. PubMed PMID: 25096877; PubMed Central PMCID: PMCPMC4128354.
145. Datsenko KA, Wanner BL. One-step inactivation of chromosomal genes in Escherichia coli K-12 using PCR products. Proc Natl Acad Sci U S A. 2000;97(12):6640-5. Epub 2000/06/01. doi: 10.1073/pnas.120163297. PubMed PMID: 10829079; PubMed Central PMCID: PMCPMC18686.
146. Tschech A, Pfennig N. Growth yield increase linked to caffeate reduction in Acetobacterium woodii. Archives of Microbiology. 1984;137(2):163-7. doi: 10.1007/BF00414460.

Supplementary Information

S1 Text. Supplementary Text

Contains supplemental sections covering additional information on the taxon set compilation, a statistical exploration of all protein-coding genes, genomes and orthologs in Set-R, details on the method and workflow of the ESGC prediction, and provides additional results and discussions for the predicted $ESGCs_{ACB}$ including several clusters not discussed in the main manuscript.

(.docx)

S1 Fig. In Set-R there is a significant difference in the number of coding sequences between the ACB clade members and non-members.

(A) Comparison of the number of coding sequences (CDS) per genome between members and non-members of ACB clade across *Acinetobacter*. It reveals a significant difference. ACB clade members, on average, contain 14% more protein coding genes. (B) Correlation matrix for a range of summary statistics on genome level across SET-R. Colored cells indicate value of spearman correlation coefficient [-1,1]. The descriptive statistics analyzed are explained in S2 Table. (C) Phylogenetic diversity of the orthologous groups (OGs) calculated from the sum of branch lengths of the subtree spanned by the taxa represented in an OG**.** This distribution contrasts the taxa belonging to the ACB clade vs. the total phylogenetic diversity. Data points are colored black if the corresponding OG belongs to the set of genus-wide core genes that were also used for phylogeny reconstruction. OGs represented closer to the upper left corner are especially interesting as they are approaching ubiquitous presence within the ACB clade but are rare in the rest of the genus (colored orange for illustrative purposes).

(PDF)

S2 Fig. Majority-rule consensus phylogeny of 232 Acinetobacter strains represented in SET-R.

A high resolution image of the majority-rule consensus dendrogram of the Set-R taxa as shown in Fig 2A. Branches supported by only two out of three partition trees are indicated with dashed lines, branches supported by only one partition are not resolved. Leaf labels colored in green indicate changed species assignments. Such changes can either (i) correct (i.e. the original species assignment was at odds with the species assignment based on phylogenetic and ANI evidences), (ii) newly specify (i.e. the original species assignment was set to "unknown" (sp.)) or (iii) de-specify (the original species assignment could not be confirmed by phylogenetic evidences, and no alternative assignment was possible. The species label was set to "sp.") the species assignments as retrieved from NCBI RefSeq at the time of download.

(PDF)

S3 Fig. Maximum likelihood (ML) tree for Set-F based on partition 1 of the core gene set (296 proteins).

Branch labels denote percent bootstrap support. The newick strings for the ML trees from all three partitions are given in S3 Data. A high-resolution figure of the consensus tree is provided in S9 Fig.

(PDF)

S4 Fig. Hierarchically clustered ANIm heatmap across Set-R combined with phylogenetic information reveals unknown species diversity within the ACB clade.

The figure shows the color-graded average nucleotide identity (ANIm, all vs all) of the genomes across SET-R (both axes). Strains with high genomic identity generate clusters of

high sequence identity (>95%: increasingly saturated red; 95%: white, <95%: saturating blue) along the diagonal. These clusters and cutoffs are typically used for bacterial species delineation. In the ACB clade, we observe a large and distinct cluster with 98-100% sequence identity (rounded) for the *A. baumannii* species (top left). Following the diagonal to the bottom right corner, the strains of *A. seifertii* (2, n=2) and *A. nosocomialis* (3, n=5) are clustered similarly. The percent identities decrease, for the following two clusters of genomes with mainly *A. calcoaceticus* species assignments (4 and 5). Specifically, only three pairs in cluster 4 and one pair in cluster 5 reach the species threshold ANI. Next to putatively misidentified *A. calcoaceticus*, cluster 5 features a strain of the tentative species *A. oleivorans* (strain CIP 110421) as well as the unassigned *A.* sp. WC-141 and *A.* sp. NIPH 817 suggesting the existence of undescribed species in the ACB clade. Two further genomes, here located between cluster 5 and cluster 6 are putatively mislabeled strains *A. baumannii* strain 573719 and *A. pittii* ANC 4050. These strains again potentially represent undescribed species in the ACB clade. Clusters 6 and 7 comprise the strains from *A. lactucae* and from *A. pittii*, respectively. S12 Table contains the full matrix of pairwise ANIm in a tabulated format.
(PNG)

S5 Fig. Genomic regions of all ESGC along the genome of ATCC 19606.

Graphical representations of the genomic regions for each ESGC with RD > 0 (see Methods) along the genome of ATCC 19606 with abbreviated abundance profiles and functional annotations.
(PDF)

S6 Fig. Growth of *A. baumannii* ATCC 19606, *A. calcoaceticus* DSM 30006 and *A. baylyi* on different carbon source.

A. baumannii ATCC 19606 (△), *A. calcoaceticus* (□) and *A. baylyi* ADP1 (○) were grown in

1618 mineral medium with 20 mM carnitine (A), gluconate (B) or D-malate (C) as carbon source.

1619 Each value is the mean of +/- S. E.M. of at least three independent measurements.

1620 (PDF)

1621 **S7 Fig. Ortholog abundance profiles and functional characterizations of *gdhA* and *gdhB*.**

1622 (PDF)

1623 **S8 Fig. Numbers of HOG innovations and losses at each node of the majority-rule**

1624 **consensus tree of Set-R.**

1625 A consensus tree representation of Set-R with each inner node of the tree annotated with

1626 the number of HOGs associated to it as well as the number of lost HOGs in the subsumed

1627 clade according to the rules of Dollo (+) Parsimony (see Methods). All HOGs are provided in

1628 S13 Table. The nodes are labeled with an incremental id. On the lineage of *A. baumannii* we

1629 used the following replacements in the manuscript: NODE_1 = "ACB+BR", NODE_8 =

1630 "ACB+LW", NODE_9 = "ACB+BA", NODE_10 = "ACB+HA", NODE_11 = "ACB", NODE_12 =

1631 "BNS", NODE_13 = "B". Tip labels are represented as NCBI RefSeq Identifiers. Tip labels also

1632 show unique assembly accession and, if applicable either clone type assignment or

1633 (corrected) species assignment in form of the first four letters of the species names.

1634 (PDF)

1635 **S9 Fig. Majority-rule consensus tree (dendrogram) for Set-F summarizing the information**

1636 **in the maximum likelihood trees based on the three partitions of the core gene set**.

1637 (PDF)

1638 **S10 Fig. Treemaps (1-5) of enrichment biological processes as generated by REVIGO (*cf.* S5**

1639 **Table).**

1640 (PDF)

S1 Data. Phylogenetic profiles and microsynteny plots in html format for the curated top 150 ESGCs$_{ACB}$ across Set-F as produced by the Vicinator tool.

Files can also be downloaded in zip-format via figshare:

https://figshare.com/s/caa9a6680bc90e004365 (temporary private link).

(ZIP)

S2 Data. Phylogenetic profiles and microsynteny plots in html format for ESGC$_{ACB}$-0452 and the kynurenine pathway cluster in *P. aeruginosa* across a sample of all *Proteobacteria*.

Files can also be downloaded in zip-format via figshare:

https://figshare.com/s/caa9a6680bc90e004365 (temporary private link).

(ZIP)

S3 Data. ML trees for all three partitions in newick format including support values.

Files can also be downloaded in zip-format via figshare:

https://figshare.com/s/caa9a6680bc90e004365 (temporary private link).

(ZIP)

S1 Table. Full list of genomes used in this study.

The set of assemblies represented in Set-F is provided in tabular format as extracted from NCBI RefSeq. Among other, the table lists RefSeq assembly and sample accessions, taxonomy ids (on strain and species level if available), species labels, and strain labels, assembly status, submission date, submission institute, and ftp link to resource.

(XLSX)

S2 Table. Representative genomes selected with corrections and descriptive statistics.

The subset of assemblies in Set-R is provided in tabular format. The table lists RefSeq assembly and sample accessions, taxonomy ids, species labels, and corrected labels (see main text), strain names, clone type assignments (via MLST and literature) sampling site, and

sampling year (where available) of the strains. The table further features the results of our genome sequence-specific quantitative and qualitative analyses. The descriptive statistics are described in the documents' sheet 'ColumnLegends'.

(XLSX)

S3 Table. Orthology matrix as calculated from the all vs. all orthology search across Set-R (OMA orthologous groups)

(1) The column header contains the labels of the NCBI RefSeq assembly accession of each genome. Row indices refer to the orthologous group identifier. The matrix fields contain the NCBI RefSeq protein sequence accession if an ortholog was identified and left empty otherwise. (2) List of orthologous groups identifiers constituting the core genome by our definition. These were used for the tree reconstruction

(XLSX)

S4 Table. Phylogeny-based taxonomic classifications of the genomes in Set-F into the defined clades

Consists of 15 sheets in total. Each sheet lists the NCBI RefSeq assembly accession and taxon label (species and strain label) of the genomes that were phylogenetically classified to belong to the following clades: B clade (*A. baumannii*), S clade (*A. seifertii*), NO clade (*A. nosocomialis*), BNS clade (three aforementioned), L clade (*A. lactucae*), PI clade (*A. pittii*), CA clade (*A. calcoaceticus*), CPL clade (three aforementioned), ACB clade, HA clade, BA clade, LW clade, BR clade, QI clade, and the outgroup. Genome assignments to *A. baumannii* which were at odds with its phylogenetic placement in our study are indicated by a blue line. In the same way, we highlighted assignments to *A. pittii* in light orange and *A. calcoaceticus* in dark orange.

(XLSX)

S5 Table: Results of consecutive GO term enrichment analysis

(1) shows the significantly enriched GO terms ($p_{adjusted} < 0.001$) for proteins in those HOGs at a node where an ortholog was detected in at least 50% of the subsumed taxa. If genes of the same HOG are the source for multiple enriched terms, only the most specific term (highest depth) was kept for the final results. The raw results of the GO term enrichment analysis are presented in (2). The results of the GO term enrichment analyses considering all HOGs at a node are provided in (3). Detailed explanations of the column headers are placed in the sheet 'ColumnLegends'. The test results from (3) were extracted to generate input tables for REVIGO (sheets 4-8). The resulting treemaps are shown in S10 Fig 1-5.

(XLSX)

S6 Table. ESGC identification and underlying data.

This file gives detailed information about the ESGC identification and provides the underlying data. (1) gives for each gene along the genome of *A. baumannii* ATCC 19606 the number of taxa per clade (and per international clone type) that harbor an ortholog. (2) gives, for each gene, the input vector used for the dissimilarity calculations, the individual thresholds (5^{th} percentile) and, as an example, the calculated dissimilarity between each gene and the gene immediately upstream. The full matrix containing all pairwise dissimilarity calculations for the prediction of clusters is deposited on figshare [10.6084/m9.figshare.16910974, https://figshare.com/s/caa9a6680bc90e004365 (temporary private link)]. (3) lists the identified graph components along with abundance statistics (median of the proteins in a component) across the clades (both absolute and relative), retention difference between ACB vs. non-ACB (RD), and CCD scores. (4) lists detailed contextual information for the components including all functional annotations from various sources. Detailed explanations of the

column headers for all tables are placed in the sheet 'ColumnLegends'.

(XLSX)

S7 Table. Summary statistics of collected experimental evidence found in the literature for the assimilation of >100 potential carbon sources for *A. baumannii*.

(XLSX)

S8 Table. List of all non-ACB genomes across Set-R that harbor $ESGC_{ACB}$ 0016 including meta information regarding sampling and isolation.

(PDF)

S9 Table. Assembly accessions and species/strain labels for the *Proteobacteria* sample (n=1363).

(XLSX)

S10 Table. List of primers used for Ab04 mutant deletions Δkyn mutant strains.

(XLSX)

S11 Table. In silico MLST classifications of the genomes in Set-F.

(1) Results are in of Oxford-scheme and (2) of Pasteur-scheme typing. Sheets (3-10) list NCBI RefSeq assembly accession and strain labels for all genomes in the *A. baumannii* clade where the MLST classification allowed a mapping to one of the 8 international clone types.

(XLSX)

S12 Table. Raw values of the pairwise ANIm comparisons shown in S4 Fig.

(XLSX)

S13 Table. Hierarchical orthology matrix as calculated from the all vs. all orthology search across Set-R along the phylogenetic tree (OMA hierarchical orthologous groups, HOGs).

1734 The column header contains the labels of the NCBI RefSeq assembly accession of each
1735 genome. The second column (LCA) indicates the associated inner node of the HOG in the
1736 reconstructed phylogenetic tree. The values either refer to the node label on the lineage of
1737 *A. baumannii* or, if the node is not on lineage, an incremental node id. The corresponding
1738 nodes together with summary statistics are provided in S8 Fig. Row indices refer to the
1739 hierarchical orthologous group ID. The matrix fields contain the NCBI RefSeq protein
1740 sequence accession if an ortholog was identified otherwise they are left empty. (2) lists the
1741 identifiers of HOGs with prevalence in at least 231 genomes. These were used for the
1742 definition of core components during cluster identification
1743 (XLSX)

1744 **S14 Table. Results of BLAST search for homologues of the QS cluster against non-**
1745 ***Acinetobacter* genomes.**
1746 (XLSX).

1747